

A Role for PGC-1 α in Transcription and Excitability of Neocortical and Hippocampal Excitatory Neurons

L. J. McMeekin,^{a,b} A. F. Bartley,^c A. S. Bohannon,^c E. W. Adlaf,^c T. van Groen,^b S. M. Boas,^b S. N. Fox,^b P. J. Detloff,^d D. K. Crossman,^e L. S. Overstreet-Wadiche,^c J. J. Hablitz,^c L. E. Dobrunz,^c and R. M. Cowell^{a,b,*}

^a Department of Neuroscience, Drug Discovery Division at Southern Research, Birmingham, AL 35205, USA

^b Department of Cell, Developmental and Integrative Biology, University of Alabama at Birmingham, Birmingham, AL 35294, USA

^c Department of Neurobiology, University of Alabama at Birmingham, Birmingham, AL 35294, USA

^d Department of Biochemistry and Molecular Genetics, University of Alabama at Birmingham, Birmingham, AL 35294, USA

^e Department of Genetics, University of Alabama at Birmingham, Birmingham, AL 35294, USA

Abstract—The transcriptional coactivator peroxisome proliferator-activated receptor γ coactivator-1 α (PGC-1 α) is a critical regulator of genes involved in neuronal metabolism, neurotransmission, and morphology. Reduced PGC-1 α expression has been implicated in several neurological and psychiatric disorders. An understanding of PGC-1 α 's roles in different cell types will help determine the functional consequences of PGC-1 α dysfunction and/or deficiency in disease. Reports from our laboratory and others suggest a critical role for PGC-1 α in inhibitory neurons with high metabolic demand such as fast-spiking interneurons. Here, we document a previously unrecognized role for PGC-1 α in maintenance of gene expression programs for synchronous neurotransmitter release, structure, and metabolism in neocortical and hippocampal excitatory neurons. Deletion of PGC-1 α from these neurons caused ambulatory hyperactivity in response to a novel environment and enhanced glutamatergic transmission in neocortex and hippocampus, along with reductions in mRNA levels from several PGC-1 α neuron-specific target genes. Given the potential role for a reduction in PGC-1 α expression or activity in Huntington Disease (HD), we compared reductions in transcripts found in the neocortex and hippocampus of these mice to that of an HD knock-in model; few of these transcripts were reduced in this HD model. These data provide novel insight into the function of PGC-1 α in glutamatergic neurons and suggest that it is required for the regulation of structural, neurosecretory, and metabolic genes in both glutamatergic neuron and fast-spiking interneuron populations in a region-specific manner. These findings should be considered when inferring the functional relevance of changes in PGC-1 α gene expression in the context of disease. © 2020 IBRO. Published by Elsevier Ltd. All rights reserved.

Key words: transcription, PGC-1 α , behavior, pyramidal neurons, electrophysiology.

INTRODUCTION

Reductions in the expression of peroxisome proliferator activated receptor γ coactivator-1 alpha (PGC-1 α) or polymorphisms in the gene encoding PGC-1 α have been implicated in the progression and/or onset of neurodegenerative disorders including Alzheimer's disease (Qin et al., 2009; Gong et al., 2013; Robinson

et al., 2014), Amyotrophic Lateral Sclerosis (Thau et al., 2012; Eschbach et al., 2013; Bayer et al., 2017; Dervishi et al., 2018), Parkinson's Disease (St-Pierre et al., 2006; Ebrahim et al., 2010; Zheng et al., 2010; Clark et al., 2011; Pacelli et al., 2011; Shin et al., 2011; O'Donnell et al., 2014; Eschbach et al., 2015; Su et al., 2015; Jiang et al., 2016; Soyak et al., 2018), and Huntington's Disease (HD) (Cui et al., 2006; Weydt et al., 2006, 2009; Okamoto et al., 2009; Taherzadeh-Fard et al., 2009; Chaturvedi et al., 2010; Ramos et al., 2012; 2014; Török et al., 2015). Normally, PGC-1 α enhances gene transcription by facilitating interactions between co-expressed transcription factors and regulators in a given cell.

As these transcription factors and regulators are expressed in a cell-specific manner, deficiency of PGC-1 α is likely to result in different effects depending on the

*Corresponding author at: Drug Discovery Division, Southern Research, 2000 9th Avenue South, Birmingham, AL 35205, USA. E-mail address: rcowell@southernresearch.org (R. M. Cowell).

Abbreviations: Aps, action potentials; EGTA, ethylene glycol-bis(β -aminoethyl ether)-N,N,N',N'-tetraacetic acid; EMX-1, empty spiracles homeobox 1; fPSPs, field postsynaptic potentials; FV, fiber volley; GCs, granule cells; HD, Huntington Disease; HEPES, 4-(2-hydroxyethyl)-1-piperazineethanesulfonic acid; MSNs, medium spiny neurons; PFA, paraformaldehyde; PGC-1 α , proliferator-activated receptor γ coactivator-1 α ; PNs, pyramidal neurons; PV, protein parvalbumin; ROI, region-of-interest.

cell population in which it is occurring. Understanding the cellular specificity of PGC-1 α -dependent transcription under normal conditions will enhance understanding of the contribution of its loss in expression and/or function to disease.

Our lab and others have shown that PGC-1 α null mice exhibit robust motor deficits (Lin et al., 2004; Leone et al., 2005; Lucas et al., 2012, 2014b) and vacuoles throughout the brain, particularly in neocortex and striatum (Lin et al., 2004; Lucas et al., 2012; Szalardy et al., 2013). Reductions in metabolic (Lin et al., 2004; Cowell et al., 2009; Lucas et al., 2014a), vesicular release and axonal stabilizing transcripts (Lucas et al., 2014a) are associated with reduced inhibition in the PGC-1 α null motor neocortex (Dougherty et al., 2014a) and reduced intrinsic excitability of parvalbumin-positive interneurons (PV-INs) (Dougherty et al., 2014a). We have found that PV-INs rely heavily on PGC-1 α for the expression of the calcium buffering protein parvalbumin (PV) (Lucas et al., 2014a). However, selective deletion of PGC-1 α from PV-INs fails to recapitulate vacuolization or the transcriptional and electrophysiological deficits seen in the null neocortex (Lucas et al., 2014a). While these animals exhibit impaired long-term memory (Lucas et al., 2014a) and deficits in hippocampal circuit function and nest building behavior (Bartley et al., 2015), motor function is maintained (Lucas et al., 2014a). These findings suggest that dysfunction in other cell types contributes to the transcriptional and behavioral phenotype of PGC-1 α null mice, and that these neurons could be affected by PGC-1 α deficiency in disease.

Previous studies have reported moderate expression of PGC-1 α in neocortical and hippocampal pyramidal neurons (PNs) in the rodent brain (Cowell et al., 2007; Cheng et al., 2012; Jiang et al., 2013), and PV-INs have reduced glutamatergic input from PNs in the PGC-1 α null neocortex (Dougherty et al., 2014a), suggesting that PGC-1 α is required for normal PN function. Deletion of PGC-1 α from CAMKII α -positive neurons results in neocortical and striatal vacuoles (Ma et al., 2010). Since CAMKII α is enriched in striatal medium spiny neurons (MSNs) and neuronal populations within the amygdala (Minichiello et al., 1999) in addition to PNs, and expressed even in some interneuron populations (Saunders et al., 2018), the sole contributions of neocortical and hippocampal glutamatergic dysfunction to abnormalities in PGC-1 α null mice are unclear.

Here, we show that deletion of PGC-1 α from non-interneuron cell populations in the forebrain accounts for ~80% of total neocortical PGC-1 α mRNA. Deletion of PGC-1 α from these populations caused novelty-induced hyperactivity, reduced expression of axonal stability gene *Nefh* and synchronous release transcripts *Syt2* and *Cplx1*, and region-specific decreases in metabolic gene expression. These gene expression changes were accompanied by increased neuronal excitability in the neocortex and hippocampus without motor impairment or vacuolizations observed in whole body PGC-1 α null mice. These gene expression changes were not observed in the neocortex and hippocampus in an HD mouse model, suggesting that PGC-1 α -dependent transcriptional programs are not disrupted in these mice.

Together, these findings confirm a role for PGC-1 α in the regulation of genes involved in neurotransmitter release and neuronal structure and suggest a specific role for PGC-1 α with respect to cell-population and region, providing insight into the consequences of PGC-1 α deficiency in disease.

EXPERIMENTAL PROCEDURES

Animals

All experimental procedures were approved by the Institutional Animal Care and Use Committee of the University of Alabama at Birmingham and conducted in accordance with the *Guide for the Care and Use of Laboratory Animals* adopted by the U.S. National Institutes of Health. Males and females between the ages of 3–5 months or 1 year were used for experiments. Unless otherwise noted, littermates expressing Cre-recombinase without the floxed allele were used as controls as in our previous publications; the floxed allele alone had no effect on behavior or gene expression (see results). All mice were maintained on a C57BL6/J genetic background and housed two to five per cage at 26 \pm 2 $^{\circ}$ C with food and water *ad libitum*.

PN-specific deletion of PGC-1 α was achieved by crossing mice with LoxP sites flanking exons 3–5 of the *PPARGC1A* gene (Lin et al., 2004) (gift from Bruce Spieglerman, Dana-Farber Cancer Institute, Boston, MA, USA) with those expressing Cre-recombinase driven by the empty spiracles homeobox 1 (EMX-1) promoter (JAX005628). EMX-1Cre;PGC-1 α ^{+/*fl*} female mice were crossed with WT;PGC-1 α ^{+/*fl*} male mice to yield EMX-1Cre;PGC-1 α ^{+/*+*}, EMX-1Cre;PGC-1 α ^{+/*fl*}, and EMX-1Cre;PGC-1 α ^{*fl/fl*} littermates.

Neocortical and hippocampal cDNA from an HD knock-in mouse line for transcriptional studies was generated as described (Kumar et al., 2016) to assess neocortical and hippocampal involvement of mutant huntingtin (mhtt) in PGC-1 α -dependent pathways. Mice 5–7 months of age homozygous for mouse huntingtin knock-in alleles with 50, 100, 150 (144–164) and 200 (194–211) CAGs were compared alongside wildtype (HDQ7/7) controls. Throughout the text, genotypes indicating repeat length and homozygosity are indicated as 50/50, 100/100, etc. We have previously replicated reductions in striatal *Drd2* transcript, a hallmark of HD pathogenesis, from these knock-in animals (McMeekin et al., 2018).

Small molecule fluorescent in situ hybridization (SM-FISH)

SM-FISH was performed as previously described (McMeekin et al., 2018) using the RNAscope Multiplex Fluorescent assay (Advanced Cell Diagnostics, Newark, CA, USA) according to the manufacturer's instructions. Mice at 4–6 months of age (localization studies) or 8 months (recombination studies) were briefly anesthetized with isoflurane and decapitated. Brains were removed and frozen with powdered dry ice and stored at -80° C. Tissue was cryosectioned at 20 μ m sections,

collected on SuperFrost Plus slides (Thermo Fisher Scientific) and kept on dry-ice. Samples were fixed in 4% prechilled paraformaldehyde (PFA) followed by dehydration in ethanol and pretreatment in protease IV (Advanced Cell Diagnostics). Probes were custom-designed to recognize exons 3–5 of PGC-1 α (Catalog #515871, Advanced Cell Diagnostics). Colocalization studies were performed using probes for parvalbumin (Pvalb), vesicular glutamate transporter 1 (Vglut1; to label excitatory neurons), and gap junction protein alpha 1 (Gja1; to label astrocytes) (Catalog #421931, 416631, and 486191, respectively; Advanced Cell Diagnostics). Tissue was incubated with a mixture of probes for 2 h at 40 °C followed by fluorescent amplification and mounting with Prolong gold antifade mounting medium containing DAPI (Thermo Fisher Scientific). Images ($n = 4$ wildtype mice/study; 2 cortical sections/mouse; 4 images/section, Bregma 0.26 mm) were captured with a Nikon A1 confocal microscope. For quantification studies, an average number of cells per animal are as follows: PV $^+$ = 131, VGLUT $^+$ = 2868, Gja1 $^+$ = 413. For confirmation of recombination, $n = 2$ animals/genotype. All settings, including laser intensity, gain, offset, and zoom, were held constant across all images. Quantification of pixel density for a given *in situ* probe was performed using ImageJ (Schneider et al., 2012). All images were set to 8 bit, and a threshold that best represented fluorescent signal was set for a given channel and applied across all compared images. Pixel density for the cell area was recorded for each region-of-interest (ROI); the cell marker defined the ROI. For each cell marker, values were averaged across the cells of each animal to generate one composite data point per animal; data are mean \pm SEM.

Transcript analyses

Quantitative PCR was performed as previously described (Lucas et al., 2012). Mice were anesthetized with isoflurane prior to decapitation. Brains were rapidly removed and microdissected brain regions were flash frozen on dry ice and stored at -80 °C until use. Tissue was homogenized in TRIzol (Thermo Fisher Scientific, Pittsburgh, PA, USA) using either a Tissue-Tearor homogenizer (Biospec, Bartlesville, OK, USA) or the Omni Bead Ruptor Homogenizer (OMNI International, Kennesaw, GA, USA), and RNA was isolated using the TRIzol/chloroform-isopropanol method following the manufacturer's instructions (Invitrogen, Carlsbad, CA, USA). RNA concentration and purity were assessed using a NanoDrop One (Thermo Fisher Scientific, Pittsburgh, PA, USA). Equivalent amounts of RNA (1 μ g) were treated with DNase I (Promega, Madison, WI, USA) at 37 °C for 30 min followed by DNase Stop solution at 65 °C for 15 min. RNA was then reverse-transcribed using the High-Capacity cDNA Reverse Transcription Kit (Thermo Fisher Scientific, Carlsbad, CA, USA). Transcripts were measured using mouse-specific primers from Applied Biosystems (Supplemental Table S1) and JumpStart Taq Readymix (Sigma, St. Louis, MO, USA) using a protocol with an initial ramp (2 min, 50 °C; 10 min, 95 °C) and 40 subsequent cycles (15 s, 95 °C; 1 min, 60 °C). Relative concentration of transcript was calculated in comparison

to a standard curve generated from pooled cDNA samples and then diluted (1:5, 1:10, 1:20, 1:40; calibrator method). In the EMX-1Cre transgenic mouse line, $n = 9$ –14 animals/genotype for transcriptional studies. For the HDQ knock-in line, $n = 6$ –29/genotype for neocortical and $n = 7$ –22/genotype for hippocampal assays. These values were then normalized to beta-actin or 18S expression and reported as ratio to control samples \pm SEM.

Western blot

Assays were performed as previously described (Lucas et al., 2014). Cortical and hippocampal samples were collected ($n = 7$ –8/genotype), frozen on dry-ice, and stored at -80 °C until use. Samples were placed in RIPA buffer (150 mM NaCl, 50 mM Tris, 1% Triton X-100, 0.1% SDS, 0.5% deoxycholic acid, pH 8.0), and homogenized using the Omni Bead Ruptor Homogenizer (OMNI International). Total protein concentration was determined with a bicinchoninic acid protein assay kit (Thermo Fisher Scientific), and absorbance was measured at 540 nm. Protein was denatured in sample buffer (62.5 mM Tris-HCl, 20% glycerol, 2% SDS, 5% β -mercaptoethanol, 1 mg/mL bromophenol blue; pH 6.8) at 95 °C. Equivalent amounts of protein were loaded into 4–20% Mini-PROTEAN® TGX™ precast gels (Bio-Rad, Hercules, California, USA). An interblot control sample was loaded onto both gels within an experiment. Protein was transferred onto nitrocellulose membranes and blocked for 1 h with 5% milk in Tris-buffered saline (TBS; pH 7.6) with 1% Tween (TBS-T). Membranes were then probed with an antibody against synaptotagmin 2/Syt2 [znp-1, Zebrafish International Resource Center, Eugene, OR, USA; (Fox and Sanes, 2007; Su et al., 2010)] in 5% IgG-free bovine serum albumin (BSA; Jackson ImmunoResearch) in TBS-T overnight at 4 °C. Following incubation in HRP-conjugated secondary antibodies (Invitrogen) in 5% milk in TBS-T for 1 h at room temperature, membranes were placed in Immobilon® Crescendo HRP substrate (Millipore) and imaged using the ChemiDoc MP Imaging System (Bio-Rad). Membranes were then washed and re-probed for actin (MAB1501, Millipore) in 5% milk in TBS-T for 1 h at room temperature and developed as before. The optical density of bands was calculated after background subtraction using Image Studio Lite (LI-COR, Lincoln, NE, USA). All bands were normalized to the interblot control band, then to actin, and expressed as mean optical density \pm SEM.

Immunohistochemistry

Immunofluorescence was conducted as previously described (Lucas et al., 2014a). Animals were anesthetized with isoflurane and perfused intracardially with cold PBS and 4% PFA in PBS. Brains were then removed, postfixed in 4% PFA for 24–72 h, and cryoprotected in graded sucrose (5–20%). Brains were embedded in 2:1 20% sucrose and Tissue-Tek O.C.T. compound (Sakura Finetek, Torrance, CA, USA) and stored at -80 °C. Tissue was cryosectioned at 30 μ m, mounted onto charged slides (Thermo Fisher Scientific),

and allowed to dry overnight before freezing at -80°C . Slides were washed in PBS prior to blocking for 1 h with 10% serum from the host of the secondary antibody in PBS. For antigen retrieval, slides were incubated in citrate buffer (10 mM citric acid, pH 6.0) at 37°C for 10 min, then for 20 min at room temperature. Slides were then incubated with the primary antibody (anti-Nefh, Abcam; anti-Syt2, ZIRC) in 5% serum and 3% BSA in 0.3% Triton-X100 (Sigma-Aldrich, St. Louis, MO, USA) in PBS at 4°C overnight.

Slides were washed the next day and incubated with the corresponding fluorescence-conjugated secondary antibodies (Jackson ImmunoResearch, West Grove, PA, USA; Invitrogen, Thermo Fisher Scientific) for 1 h at room temperature in 5% serum from the host of the secondary antibody in PBS with 3% BSA and 0.3% Triton-X100. Following washes, sections were coverslipped using Prolong Antifade Gold with DAPI (Invitrogen) and stored at 4°C . Images (Bregma 0.26 mm) were captured with a Leica confocal microscope. All confocal settings, including laser intensity, gain, offset, and zoom, were held constant across all groups for a given analysis. For Syt2 pixel density quantification ($n = 2\text{--}5$ images/mouse, 3 mice/genotype), integrated density was obtained and compared across images using ImageJ. Data for ROIs is presented as mean \pm SEM.

Neocortical electrophysiology

Mice were anesthetized with isoflurane and decapitated. The brain was removed and immediately placed in ice-cold oxygenated (95% $\text{O}_2/5\%$ CO_2 , pH 7.4) cutting solution consisting of (in mM): 135 N-Methyl-D-glucamine, 1.5 KCl, 1.5 KH_2PO_4 , 23 choline HCO_3 , 0.4 ascorbic acid, 0.5 CaCl_2 , 3.5 MgCl_2 and 25 D -glucose (Tanaka et al., 2008). Coronal brain slices (300 μm thick) were made using a Pelco 3000 vibratome (Ted Pella Inc, Redding, CA, USA). Slices were stored in saline containing (in mM) 124 NaCl, 2.5 KCl, 10 D -glucose, 26 NaHCO_3 , 2.5 CaCl_2 , 1.3 MgCl_2 at room temperature until recording.

Individual slices were transferred to a submerged recording chamber mounted on the stage of a Zeiss AxioExaminer D1 microscope (Carl Zeiss Inc, Thornwood, NY, USA), equipped with Dodt contrast optics, a $40\times$ -water immersion lens, and infrared illumination to view neurons in the slices. The recording chamber was continuously perfused with oxygenated saline (3 ml/min at 30°C). Whole-cell voltage-clamp recordings were obtained using a Patch Clamp PC-505A amplifier (Warner Instrument Co., Hamden, CT, USA). Patch electrodes had an open tip resistance of 3–5 $\text{M}\Omega$ when filled with an intracellular solution containing (in mM): 125 K-gluconate, 10 KCl, 10 HEPES, 10 creatine- PO_4 , 2 Mg-ATP, 0.2 Na-GTP, 0.5 EGTA, which had an adjusted pH and osmolarity of 7.3 and 285, respectively. Tight seals of 1 $\text{G}\Omega$ or greater were obtained under visual guidance before breaking into whole-cell mode. Layer V pyramidal neurons were identified by their morphology and distance from the pial surface. Identity of patched cells was confirmed by analysis of the cells' responses to hyperpolarizing and

depolarizing current injection steps. Bicuculline-methiodide (Abcam) and tetrodotoxin-citrate (Sigma) were diluted from stock solutions to final concentrations in artificial cerebral spinal fluid (ACSF). For intrinsic properties, 8 EMX-1Cre:PGC-1 $\alpha^{+/+}$ animals (1–6 cells/animal, 20 cells total) and 4 EMX-1Cre:PGC-1 $\alpha^{\text{fl/fl}}$ animals (1–5 cells/animal, 12 cells) were analyzed. For mEPSCs, $n = 8\text{--}10$ cells/genotype; sEPSCs $n = 10\text{--}14$ cells/genotype.

Signals were acquired using Clampex 8.2 software and a Digidata 1322A interface (Molecular Devices, San Jose, CA, USA). Responses were digitized at 10 kHz, filtered at 5 kHz, and analyzed using Mini Analysis Program 6.0.3 (Synaptosoft, Fort Lee, NJ, USA). Action potential kinetics were calculated from the first spike fired at rheobase. Intrinsic properties were calculated from recordings of neurons at resting membrane potential in current clamp configuration. 800 ms current steps were injected in 50 pA intervals up to 100 pA above rheobase. Firing rate and spike adaptation were calculated from action potentials (APs) fired at a current amplitude double that of each cell's rheobase. Cells were voltage clamped at -70 mV to determine spontaneous and miniature event properties. The amplitude and instantaneous frequencies of events were obtained from a data acquisition period lasting 3 min to determine spontaneous and miniature event properties.

Dentate electrophysiology

Mice were anesthetized and perfused intracardially with cold cutting solution containing (in mM): 110 choline chloride, 25 D -glucose, 2.5 MgCl_2 , 2.5 KCl, 1.25 Na_2PO_4 , 0.5 CaCl_2 , 1.3 Na-ascorbate, 3 Na-pyruvate, and 25 NaHCO_3 . The brain was removed and 300 μm horizontal slices were taken from intermediate to ventral hippocampus on a Vibratome 3000EP or Leica VT1200S in cold cutting solution. After recovery in ACSF containing (in mM): 125 NaCl, 2.5 KCl, 1.25 NaH_2PO_4 , 2 CaCl_2 , 1 MgCl_2 , 25 NaHCO_3 , and 25 glucose, recordings were performed at 30°C in ACSF + 100 μm picrotoxin to block GABA_A receptors. Patch pipettes were filled with the following (in mM): 115 K-gluconate, 20 KCl, 4 MgCl_2 , 10 HEPES, 4 Mg-ATP, 0.3 Na-GTP, 7 phosphocreatine, 0.1 EGTA and 0.2% biocytin, pH 7.2 and 290 mOsm (2–4 $\text{M}\Omega$). Field pipettes were placed in the middle molecular layer and filled with ACSF (1–2 $\text{M}\Omega$). A patch pipette filled with 1 M NaCl (1 $\text{M}\Omega$) was used to stimulate the middle molecular layer, determined by paired-pulse depression of the EPSC response, using an isolated stimulator (Digitimer, Fort Lauderdale, FL, USA). EPSC amplitudes were normalized to the fiber volley amplitudes from simultaneously recorded fEPSPs for each cell. For dentate electrophysiology experiments, $n = 8$ cells/genotype.

CA1 electrophysiology

Mice were anesthetized with isoflurane and decapitated, and brains were rapidly removed. 400 μm thick coronal slices of hippocampus were cut on a vibrating

microtome (7000 smz; Campden Instruments Ltd., Lafayette, IN, USA). Slicing and dissection of the hippocampi were done in ice-cold (1–3 °C) cutting solution containing the following (in mM): 135 N-Methyl-D-glucamine, 1.5 KCl, 23 NaHCO₃, 0.4 ascorbic acid, 10 D-glucose, 1.5 KH₂PO₄, 0.5 CaCl₂, and 3.5 MgCl₂, bubbled with 95% O₂/5% CO₂, pH 7.35–7.45 (Tanaka et al., 2008). Hippocampal slices were placed in a holding chamber in a water bath at 35 °C for 60 min in a standard saline solution (Bartley et al., 2015) consisting of (in mM): 120 NaCl, 3.5 KCl, 0.75 CaCl₂, 4.0 MgCl₂, 1.25 NaH₂PO₄, 26 NaHCO₃, and 10 glucose, bubbled with 95% O₂/5% CO₂, pH 7.35–7.45. Slices were kept at room temperature until recording. During all CA1 electrophysiology experiments, slices were held in a submersion recording chamber perfused (3–4 mLs/min) with external recording solution (ERS). ERS is composed of the following (in mM) 120 NaCl, 3.5 KCl, 2.5 CaCl₂, 1.3 MgCl₂, 1.25 NaH₂PO₄, 26 NaHCO₃, and 10 glucose, bubbled with 95% O₂/5% CO₂, pH 7.35–7.45. The CA1 electrophysiology experiments were performed between 28 °C to 30 °C.

Hippocampal CA1 whole cell recordings

For whole cell recordings from CA1 PNs from intermediate to ventral hippocampal slices, the ERS contained 100 μM picrotoxin. Patch electrodes (4–6 MΩ) were filled with internal solution composed of the following (in mM): 125 K-gluconate, 0.5 EGTA, 2 MgCl₂, 10 KCl, 10 HEPES, 2 Na-ATP, 10 phosphocreatine-tris, and 0.2 GTP. pH was adjusted to 7.3 with KOH. CA1 PNs were initially recorded in the voltage-clamp configuration and held at –60 mV. The access resistance and holding current (<200 pA) were monitored continuously. Recordings were rejected if either access resistance or holding current increased >20% during the experiment. The resting membrane potential was determined immediately after break-in, and input resistance was measured with a 400 ms, –8 mV step from a –60 mV holding potential. To obtain intrinsic firing properties, CA1 PNs were recorded in current-clamp configuration while maintaining a holding potential of –60 ± 1 mV within 10 min of breaking into the cell. Firing frequency versus injected current plots (F–I plots) were made by measuring the initial firing frequency of a spike train evoked by a series of incremental 600-ms current steps at intervals of 25 or 50 pA. Using the 250 pA current step, CA1 PNs were classified as burst firing neurons if the average firing frequency between the first three APs was greater than 100 Hz. The spike threshold potential was defined as the membrane potential, in a 5 ms window preceding spike peak, at which the third derivative was maximum (an inflection point). The AP amplitude was calculated from the spike threshold to the peak of the AP. The AP half-width is the duration of the AP measured at the half way point of the AP amplitude. Afterhyperpolarization (AHP) was calculated from the spike threshold to the peak of the AHP. Spike amplitude adaptation and spike frequency accommodation were measured at the 500 pA current step. Spike amplitude adaptation is reported as the average ratio of the amplitudes between

the last two APs and the first AP in the spike train. Spike frequency accommodation is reported as the ratio of the frequency between the first and last two APs in the spike train. Rheobase is defined as the minimum current step required to fire a single AP. For intrinsic firing, *n* = 9 cells/genotype. For remaining intrinsic properties, *n* = 10–11 cells/genotype.

Hippocampal CA1 field recordings

For field recordings, the external recording solution also contained 50 μM D-APV (D-2-amino-5-phosphonopentanoic acid) to block NMDA receptor-mediated currents and 100 μM picrotoxin to block GABA_A receptors. Field postsynaptic potentials (fPSPs) were recorded from intermediate to ventral slices using an ERS-filled microelectrode in response to extracellular stimulation with a bipolar tungsten microelectrode (FHC, Bowdoinham, ME). Two field recording and stimulation electrodes were placed in the slice, one pair in s. radiatum and the other pair in s. lacunosum moleculare to measure the CA1 dendritic fEPSPs in response to stimulation of the Schaffer collateral and temporoammonic pathways, respectively. The stimulation intensity was adjusted to obtain 40–50% of the maximal fEPSP response. Paired-pulse stimulation at different intervals (in ms: 50, 100, 200, 500, and 1000) were applied and repeated 15–20 times for each interval at 0.1 Hz. The stimulation intensity ranged from 10 μA to 100 μA, unless otherwise noted, and the duration of stimulation was 100 μs. For the input/output curves, a stable baseline was obtained before applying a series of stimulus intensities (10 μA to 150 μA). For these experiments, *n* = 5–8 cells/genotype.

Behavioral analyses

All behavioral analyses were conducted during the lights-on period (6:00 A.M.–6:00 P.M.) with the experimenter blind to genotype. Rotarod, qualitative behavioral assays, and open field were performed as previously described (Lucas et al., 2012). The rotarod apparatus (MedAssociates, St. Albans, VT, USA) consisted of a five-station rotating rod with a computer-controlled motor-driven drum. The rotations per minute were programmed to be at an accelerating or constant speed. Animals were trained on the rotarod for four consecutive days. During the training period, animals were placed on the rotarod at an accelerating speed (2.0–20 rpm) on day 1 and at a constant speed (24 rpm) on days 2–4 for a maximum of 60 s for a total of four trials for each animal per day. On the fifth day, animals underwent two trials each at rotating speeds of 2.0–20 accelerating and 16, 20, 24, 28, and 32 fixed rpm. Each trial lasted for a maximum of 60 s, during which latency to fall was recorded. Mice were allowed to rest for at least five minutes between each trial. Prior to assessing rotarod performance on test day, mice were observed for the presence of hindlimb clasping by suspending the mouse by the tail for 15 s. Hind-limb clasping was marked present if the mouse clasped hindlimbs together or forelimb to hindlimb. Additionally, mice were observed in a holding cage for

overt signs of tremor. Sample sizes for these experiments were $n = 7$ EMX-1Cre:PGC-1 $\alpha^{+/+}$ and $n = 8$ EMX-1Cre:PGC-1 $\alpha^{fl/fl}$.

For assessment of baseline activity, animals were placed in a square open field apparatus (27.9 cm²) consisting of 48 infrared beams (MedAssociates, St. Albans, VT, USA) in a lit room for 30 min. Data were collected with Open Field Activity Software (MedAssociates, St. Albans, VT, USA) and binned into five-minute intervals over the test period. Sample sizes for these experiments were $n = 9$ EMX-1Cre:PGC-1 $\alpha^{+/+}$ and $n = 8$ EMX-1Cre:PGC-1 $\alpha^{fl/fl}$. For MK-801 studies, a separate cohort of animals was used ($n = 6, 8$); animals were injected with 0.2 mg/kg MK-801 and immediately placed in the open field chamber.

The water maze apparatus and procedure are previously described (Liu et al., 2002). A plastic blue pool, 120 cm in diameter, and a transparent round platform, 10 cm diameter, located 0.5 cm below the water surface were used. On days 1 through 5 of testing, mice were trained to find a hidden platform that was kept in a constant position. Four trials per day were conducted with starting positions at the north, south, east and west designations of the pool; the order of the starting position was different each day. Mice were given 60 s to find the platform; the trial ended when the mouse spent 10 s on the platform. Inter-trial intervals were approximately 2 min. After the end of day 5, mice were tested in a 60 s probe trial in which the escape platform was not present. During the probe trial, mice that have learned the platform position will spend more time in the quadrant of the pool where the platform was previously located. Animal tracking was recorded using EthoVisionXT video software (Noldus, Leesburg, VA, USA). Sample sizes for these experiments were $n = 6$ EMX-1Cre:PGC-1 $\alpha^{+/+}$ and $n = 11$ EMX-1Cre:PGC-1 $\alpha^{fl/fl}$.

The zero maze consisted of a ring-shaped corridor, 70 cm in diameter and 40 cm above the ground. The maze was divided into four equal parts; two opposing quadrants had two 15 cm high nontransparent walls and the remaining two opposing quadrants had walls that were 0.5 cm high. Mice were placed in the maze and observed for 4 min, using EthoVisionXT video tracking software (Noldus, Leesburg, VA, USA). Sample sizes for these experiments were $n = 11$ EMX-1Cre:PGC-1 $\alpha^{+/+}$ and $n = 12$ EMX-1Cre:PGC-1 $\alpha^{fl/fl}$.

Analysis of previously published transcriptional datasets

To identify novel transcripts expressed by excitatory neurons in the mouse neocortex, we compared data published by (Mo et al., 2015) of transcripts enriched in mouse excitatory neurons (“Exc” dataset; GEO: GSE63137) to our lab’s previously reported list of genes responsive to PGC-1 α overexpression in cell culture (Lucas et al., 2014). TopHat version 2.1.1 was used to align the fastq files to the UCSC mm10 reference genome; transcript abundance was estimated with Cufflinks version 2.2.1, and Cuffdiff was used to perform the pairwise differential expression analysis. p and q value cutoffs were set at < 0.05 . Overlap between transcripts enriched

in excitatory neurons and transcripts induced by PGC-1 α overexpression (Lucas et al., 2014a) was determined using Venny 2.1 (Oliveros J.C. 2007–2015).

Data analyses

All statistical analyses were conducted using IBM SPSS Statistics software or GraphPad Prism, and data are represented as the mean \pm SEM. For parametric models, the assumption of normality was examined with a Kolmogorov-Smirnov test and Q-Q plots. If these assumptions were violated, non-parametric tests were used. For SM-FISH, data were analyzed using a one-way ANOVA followed by Tukey’s multiple comparisons. For transcript analyses, all data were analyzed using non-parametric Kruskal-Wallis test followed by Dunn’s multiple comparisons or a Mann-Whitney comparison. A one-tailed t -test or Mann-Whitney was used based on an *a priori* hypothesis that measured transcripts would be reduced by a loss of PGC-1 α , and are indicated as such in the results section. For repeated measures (RM)-ANOVA, assumptions of homogeneity of variances and sphericity (for more than two levels of the repeated factor) were examined with a Levene’s (based on median) and Mauchly’s test, respectively. When necessary, sphericity was corrected with a Huynh-Feldt adjustment of the degrees of freedom. For significant main effects and/or interactions, post-hoc analyses were conducted using the Holm-Bonferroni method. All cumulative probability plots were analyzed using the Kolmogorov-Smirnov test. For CA1 intrinsic burst firing classification, data were analyzed using a two-sided Fisher’s Exact test. For Open Field MK801 data, one animal in the control group was removed as an outlier due to excessive activity that was more than three standard deviations above the mean (for all animals, regardless of genotype). The same holds true for outliers removed from fiber volley assessment in the temporoammonic pathway; these outliers were removed for being more than three standard deviations below the mean. For transcriptional analyses, outliers were identified using the ROUT method with Q set at 1%.

RESULTS

Previous work from our laboratory demonstrated that GABAergic neurons express high levels of PGC-1 α , and that the expression of the calcium-binding protein parvalbumin (PV/Pvalb) in fast-spiking neocortical neurons (PV-INs) is dependent on its expression (Cowell et al., 2007; Lucas et al., 2010, 2014a). Enrichment of PGC-1 α transcript and its responsive genes in PV-INs has been recently confirmed by unbiased transcriptional profiling of interneuron populations (Paul et al., 2017); indeed, our own analysis of data generated from the isolation of RNA selectively from PV-INs and PNs (Mo et al., 2015) demonstrates the enrichment of PGC-1 α and its target genes in PV-INs with respect to the entire neocortex and to PNs. However, our studies demonstrated that only approximately 20% of the PGC-1 α mRNA in the neocortex could be attributed to expression of PV-INs (Lucas et al., 2014a), implying expression

and possible function in non-PV-expressing neuronal populations. One previous study suggested expression of PGC-1 α in PNs of the neocortex (Jiang et al., 2013). To measure PGC-1 α gene expression in neocortical PNs, we used single-molecule fluorescent *in situ* hybridization (SM-FISH) to measure the expression of PGC-1 α in layer V and layer II/III PNs of the mouse neocortex (Vglut1+), with comparison to PV-INs (Pvalb+) and astrocytes (Gja1+) (Fig. 1A). Pixel density per region-of-interest (ROI) for PGC-1 α was significantly different between Pvalb+, Vglut1+ and Gja1+ cells ($F_{2,6} = 120.5$, $p < 0.0001$; one-way ANOVA). PGC-1 α pixel density was significantly enriched in Pvalb+ cells with respect to Vglut1+ and Gja1+ cells ($p = 0.0001$ and $p < 0.0001$, respectively; Tukey's multiple comparisons). Pixel density for PGC-1 α in Gja1+ cells was also significantly lower than that of Vglut1+ cells ($p = 0.0046$, Tukey's multiple comparisons; Fig. 1B).

To test the effects of cell-specific deletion of PGC-1 α in excitatory neurons of the neocortex and hippocampus, mice with LoxP sites flanking exons 3–5 of the *PPARGC1A* gene were crossed with mice expressing Cre-recombinase under the EMX-1 promoter. When Cre-recombinase is driven by the EMX-1 promoter, recombination occurs in radial glia, Cajal-Retzius cells, glutamatergic neurons, astrocytes, and oligodendrocytes (Gorski et al., 2002). Though EMX-1 is expressed in cells other than PNs, previous studies and Allen Brain Atlas images (www.brain-map.org) indicate that PGC-1 α mRNA and protein are not detectable in white matter (Cowell et al., 2007), as would be expected if PGC-1 α were expressed highly in oligodendrocytes. Additionally, data presented here indicate that more PGC-1 α expression is localized to a single PN on average compared to astrocytes. As a majority of affected cells in this line are PNs, we conclude that a majority of the transcriptional changes occurring in neocortex and hippocampus of this knockout are driven primarily by PNs. To confirm knockdown, we measured PGC-1 α transcript using primers recognizing exons 5–6 of the *PPARGC1A* gene in the neocortex and hippocampus. In the neocortex, transcript for PGC-1 α was significantly different amongst the genotypes ($H_2 = 20.9$, $p < 0.0001$) with expression being reduced in the EMX-1Cre:PGC-1 $\alpha^{fl/fl}$ neocortex compared to that of EMX-1Cre:PGC-1 $\alpha^{+/fl}$ by 33% and EMX-1Cre:PGC-1 $\alpha^{+/+}$ mice by 77% ($p = 0.024$ and $p < 0.0001$, respectively; Fig. 1C). PGC-1 α expression was also significantly reduced amongst the genotypes in the hippocampus ($H_2 = 24.26$, $p < 0.0001$); posthoc analysis revealed reductions in both EMX-1Cre:PGC-1 $\alpha^{+/fl}$ and PGC-1 $\alpha^{fl/fl}$ hippocampus (57% and 78%, respectively) compared to control ($p = 0.013$ and $p < 0.0001$, respectively) and reductions in the EMX-1Cre:PGC-1 $\alpha^{fl/fl}$ compared to PGC-1 $\alpha^{+/fl}$ ($p = 0.024$; Fig. 1D).

To validate recombination in PNs, we used SM-FISH probes specific for the transcription factor binding domain of PGC-1 α (exons 3–5) in the EMX-1Cre:PGC-1 $\alpha^{fl/fl}$ line (McMeekin et al., 2018). In the neocortex, PGC-1 α (green) overlaps with both Pvalb (red) and Vglut1 (blue) in both neocortical (Fig. 1E) and hippocampal

(Fig. 1F) pyramidal neurons (arrows) and Pvalb+ interneurons (arrowheads) in the EMX-1Cre:PGC-1 $\alpha^{+/+}$ brain. The localization of PGC-1 α to Vglut1-positive cells is lost in the EMX-1Cre:PGC-1 $\alpha^{fl/fl}$ brain; only localization to PV-INs remains (white arrowheads).

PGC-1 α regulates transcripts involved in axonal structure and synchronous neurotransmitter release

Previous work from our lab identified a set of neuronal transcripts upregulated by PGC-1 α overexpression, reduced in whole body knockouts, and reduced by selective deletion of PGC-1 α from PV-INs (Lucas et al., 2010, 2014a; Bartley et al., 2015), including synaptotagmin 2 (Syt2), complexin 1 (Cplx1) and neurofilament heavy chain (Nefh). In the present study, we found that neocortical Syt2 expression was significantly different amongst genotypes ($H_2 = 12.84$, $p = 0.0016$); posthoc analysis showed reduced expression in the EMX-1Cre:PGC-1 $\alpha^{+/fl}$ and PGC-1 $\alpha^{fl/fl}$ neocortex compared to control ($p = 0.0052$). There were also genotypic differences in Nefh expression ($H_2 = 7.86$, $p = 0.02$); transcript was significantly reduced in the EMX-1Cre:PGC-1 $\alpha^{fl/fl}$ neocortex compared to control by posthoc analysis ($p = 0.015$). There was no effect of PGC-1 α deletion on Cplx1 expression in this region ($H_2 = 3.19$, $p = 0.20$). Importantly, there was no change in expression of Pvalb ($H_2 = 0.44$, $p = 0.80$; Fig. 2A), indicating that recombination did not occur in PV-INs. Further, no differences were observed in transcript for PGC-1 α ($U_{5,5} = 12$, $p > 0.99$) or Syt2 ($U_{5,5} = 9$, $p = 0.55$) in the cortex of EMX-1Cre:PGC-1 $\alpha^{+/+}$ mice compared to WT; PGC-1 $\alpha^{fl/fl}$ mice ($n = 5$ /genotype, data not shown), showing that the changes in gene expression in this model only occur with the combination of the cre transgene and floxed alleles.

We then explored the effects of PGC-1 α deletion on these transcripts in hippocampus. Syt2 transcript was significantly different amongst the genotypes ($H_2 = 15.43$, $p = 0.0004$), with posthoc analysis revealing reductions in the EMX-1Cre:PGC-1 $\alpha^{+/fl}$ and PGC-1 $\alpha^{fl/fl}$ hippocampi compared to control ($p = 0.0058$ and $p = 0.0006$, respectively). Nefh was similarly reduced ($H_2 = 8.29$, $p = 0.016$); transcript was significantly less in the EMX-1Cre:PGC-1 $\alpha^{+/fl}$ hippocampus compared to control by posthoc analysis ($p = 0.014$; Fig. 2B). Similar to what was observed in the neocortex, Cplx1 ($H_2 = 4.50$, $p = 0.11$) and Pvalb ($H_2 = 3.22$, $p = 0.20$) were unaffected by a loss of PGC-1 α in PNs.

PGC-1 α deletion has more robust effects on metabolic gene expression in hippocampus than in neocortex

PGC-1 α is well-known as a regulator of transcripts involved in mitochondrial function and energy production (Spiegelman, 2007; Wareski et al., 2009; Scarpulla, 2011). Our lab has identified a set of metabolic targets that are upregulated over twofold by PGC-1 α overexpression *in vitro* and *in vivo*, and significantly reduced in the PGC-1 α null neocortex (Lucas et al., 2014a). To deter-

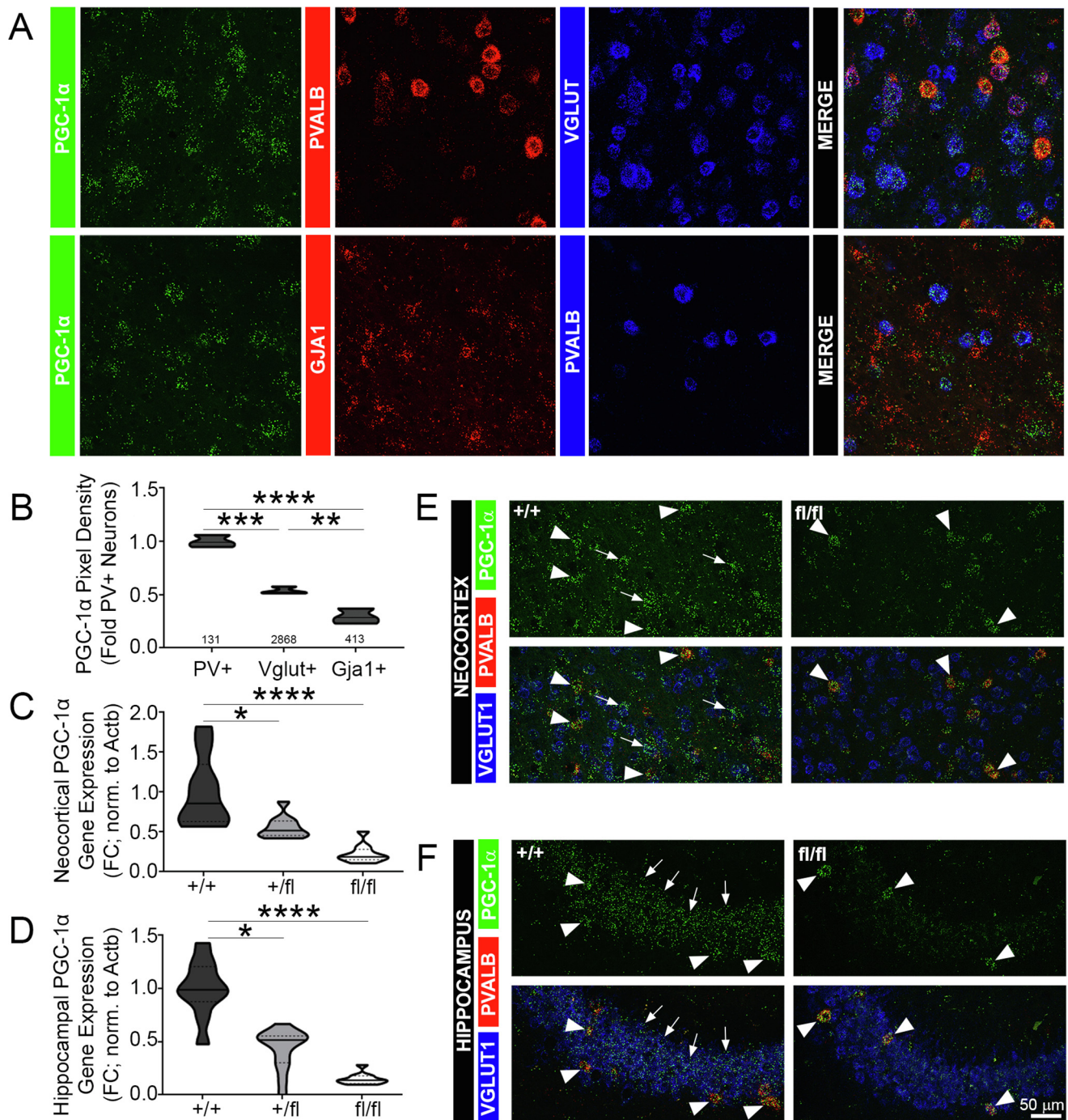
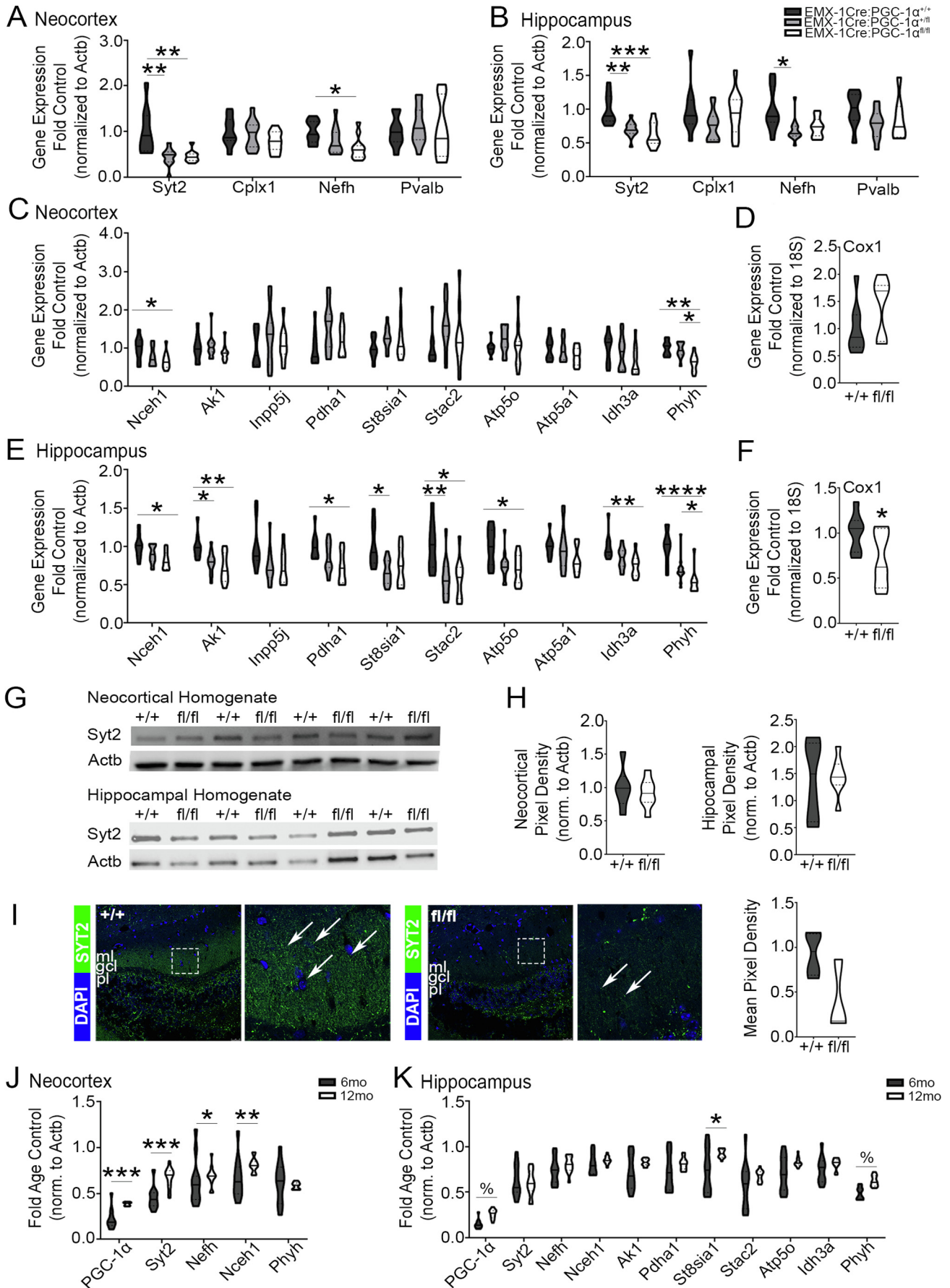


Fig. 1. EMX-1Cre-mediated deletion of PGC-1 α in neocortical and hippocampal PN. **(A)** Fluorescent *in situ* hybridization (sm-FISH) demonstrates localization of PGC-1 α to PV-INs (Pvalb, red, upper panel), PNs (Vglut1, white), and astrocytes (Gja1, red, lower panel) in wildtype cortex at 5 months of age. **(B)** Quantification of pixel density reveals significant differences in PGC-1 α expression in astrocytes, PNs, and PV-INs. $n = 4$ wildtype mice/study; 2 cortical sections/mouse; 2 images/section. Average number of cells/animal: PV = 131, VGLUT = 2868, Gja1 = 413. **(C)** PGC-1 α mRNA expression is reduced in the EMX-1Cre;PGC-1 $\alpha^{+/fl}$ and PGC-1 $\alpha^{fl/fl}$ mice in the neocortex ($n = 9$ EMX-1Cre;PGC-1 $\alpha^{+/+}$, $n = 10$ –12 EMX-1Cre;PGC-1 $\alpha^{+/fl}$, $n = 9$ –11 EMX-1Cre;PGC-1 $\alpha^{fl/fl}$) and **(D)** hippocampus ($n = 9$ –10 EMX-1Cre;PGC-1 $\alpha^{+/+}$, $n = 14$ EMX-1Cre;PGC-1 $\alpha^{+/fl}$, $n = 11$ EMX-1Cre;PGC-1 $\alpha^{fl/fl}$). FISH confirms the expression of PGC-1 α (green) localized to PV-INs (red; arrowheads) and PNs (blue; arrows), with PN coexpression absent in the EMX-1Cre;PGC-1 $\alpha^{fl/fl}$ **(E)** neocortex and **(F)** hippocampus. $n = 2$ /genotype.* $p < 0.05$; ** $p < 0.01$; *** $p < 0.001$, **** $p < 0.0001$. Data are presented as mean \pm SEM or median \pm interquartile range. (For interpretation of the references to colour in this figure legend, the reader is referred to the web version of this article.)

mine the contribution of PGC-1 α deletion in neocortical PNs to the reduction of these genes in the null neocortex, we measured these transcripts in the conditional knockout

line. Both *Nceh1* ($H_2 = 6.59$, $p = 0.037$) and *Phyh* ($H_2 = 12.11$, $p = 0.0023$) were reduced in the EMX-1Cre;PGC-1 $\alpha^{fl/fl}$ neocortex compared to controls as



revealed by posthoc analysis ($p = 0.032$ and $p = 0.0058$, respectively). Posthoc analysis also revealed that *Phyh* was reduced in the EMX-1Cre:PGC-1 $\alpha^{fl/fl}$ compared to EMX-1Cre:PGC-1 $\alpha^{+/fl}$ neocortex ($p = 0.014$). The remaining unaffected transcripts were as follows (Fig. 2C): *AK1* ($H_2 = 4.14$, $p = 0.13$), *Inpp5j* ($H_2 = 0.96$, $p = 0.62$), *Pdha1* ($H_2 = 4.31$, $p = 0.12$), *St8sia1* ($H_2 = 2.59$, $p = 0.27$), *Stac2* ($H_2 = 5.63$, $p = 0.06$), *ATP5o* ($H_2 = 2.50$, $p = 0.29$), *ATP5a1* ($H_2 = 2.44$, $p = 0.29$), *Idh3a* ($H_2 = 4.60$, $p = 0.10$). These data indicate that our previously reported reduction in the mRNA of these genes in the PGC-1 α null neocortex is likely due to a loss of PGC-1 α in interneuron populations (Fig. 2C).

In contrast, the majority of these genes were reduced in knockout hippocampus (Fig. 2E). Significant reductions amongst the genotypes were found for the following transcripts by one-way ANOVA and posthoc analyses: *Nceh1* ($H_2 = 8.06$, $p = 0.018$), *AK1* ($H_2 = 10.69$, $p = 0.0048$), *Pdha1* ($H_2 = 8.44$, $p = 0.015$), *St8sia1* ($H_2 = 8.50$, $p = 0.014$), *Stac2* ($H_2 = 11.15$, $p = 0.004$), *ATP5o* ($H_2 = 7.57$, $p = 0.023$), *Idh3a* ($H_2 = 9.97$, $p = 0.0068$), and *Phyh* ($H_2 = 18.50$, $p < 0.0001$). EMX-1Cre:PGC-1 $\alpha^{+/fl}$ hippocampus showed significant differences in the following transcripts by Dunn's multiple comparisons compared to control: *AK1* ($p = 0.030$), *St8sia1* ($p = 0.014$), *Stac2* ($p = 0.008$). The following transcripts were significantly different in the EMX-1Cre:PGC-1 $\alpha^{fl/fl}$ hippocampus compared to control: *Nceh1* ($p = 0.014$), *AK1* ($p = 0.0052$), *Pdha1* ($p = 0.011$), *Stac2* ($p = 0.01$), *Atp5o* ($p = 0.035$), *Idh3a* ($p = 0.0048$), *Phyh* ($p < 0.0001$). There was also a significant reduction in *Phyh* transcript in the EMX-1Cre:PGC-1 $\alpha^{fl/fl}$ hippocampus compared to EMX-1Cre:PGC-1 $\alpha^{+/fl}$ hippocampus ($p < 0.05$). There was no effect of PGC-1 α deletion on *Inpp5j* ($H_2 = 5.95$, $p = 0.05$) or *ATP5a1* expression ($H_2 = 4.12$, $p = 0.13$).

Considering the roles for PGC-1 α in regulating genes which control mitochondrial biogenesis and previous reports of PGC-1 α -mediated biogenesis in primary hippocampal neurons (Cheng et al., 2012), we measured the expression of the mitochondrially-encoded gene, cytochrome c oxidase subunit I (*Cox1*) as a proxy for mitochondrial content. Due to the large reduction in mitochondrial transcripts, we expected a reduction in *Cox1*; we found that *Cox1* was significantly reduced in the conditional knockout hippocampus compared to control ($U_{8,11} = 23$, $p = 0.045$; one-tailed), while it was unchanged in the neocortex ($U_{8,8} = 19$, $p = 0.097$; one-tailed) (Fig. 2D, F).

Together, these data suggest that hippocampal PNs rely more heavily on PGC-1 α for the expression of mitochondrial genes compared to neocortical PNs.

Syt2 immunoreactivity in the dentate gyrus of the hippocampus

Syt2 was the most robustly affected PGC-1 α -dependent transcript in the neocortex and hippocampus, so we assessed *Syt2* protein levels under the *a priori* hypothesis that expression would be reduced. Representative images are shown (Fig. 2G); quantification of *Syt2* protein (Fig. 2H) revealed no differences between the EMX-1Cre:PGC-1 $\alpha^{+/+}$ or EMX-1Cre:PGC-1 $\alpha^{fl/fl}$ cortical ($t_{12} = 0.56$, $p = 0.29$; one-tailed *t*-test) or hippocampal ($t_{12} = 0.20$, $p = 0.42$; one-tailed *t*-test) homogenate.

Considering the substantial *Syt2* protein expressed by PV-INs, we predicted that subtle changes in protein expression may not be detectable with Western blotting methods. We used immunofluorescence to investigate regional changes in *Syt2* IR in the EMX-1Cre:PGC-1 $\alpha^{fl/fl}$ hippocampus. The molecular layer of the dentate gyrus, containing dendritic trees of granule cells (GCs), receives input from entorhinal PNs. *Syt2* IR (arrows) is dramatically reduced in the molecular layer of the EMX-1Cre:PGC-1 $\alpha^{fl/fl}$ mouse compared to control suggesting a reduction in *Syt2* expression in excitatory synapses onto dentate GCs. A one-tailed *t*-test revealed a nearly significant reduction in *Syt2* IR in the EMX-1Cre:PGC-1 $\alpha^{fl/fl}$ dentate compared to control ($t_4 = 1.83$, $p = 0.07$; Fig. 2I).

Though reported in the PGC-1 α null brain, vacuoles were not observed in the neocortex, hippocampus or striatum of the EMX-1Cre:PGC-1 $\alpha^{fl/fl}$ mice (data not shown). This observation would suggest that other cell types or a combinatorial deletion of PGC-1 α from multiple cell-types is a contributor to vacuolization.

Age-related changes in PGC-1 α -dependent transcripts

Given that a common feature of PGC-1 α -related neurological diseases is age-related onset of symptoms and pathology, we explored the dependence of PGC-1 α -responsive transcripts on age by comparing transcript levels that were reduced in the neocortex and hippocampus at 6 months to those measured at 1 year of age. Values were normalized to β -actin and



Fig. 2. PGC-1 α is required for the expression of transcripts involved in synchronous neurotransmitter release, axonal stabilization, and metabolism in the neocortex and hippocampus. Transcripts for neuron-specific *Syt2* and *Nefh* are significantly reduced by deletion of PGC-1 α in the (A) neocortex and (B) hippocampus at 3–5 months of age. Mitochondrial and metabolic transcripts are reduced to a greater extent in the hippocampus than the neocortex (C, E). *Cox1* expression (mitochondrially-encoded) is reduced in the conditional knockout hippocampus, while *Cox1* transcript is unchanged in the neocortex (D, F). Neocortex: $n = 9$ EMX-1Cre:PGC-1 $\alpha^{+/+}$, $n = 10$ –12 EMX-1Cre:PGC-1 $\alpha^{+/fl}$, $n = 9$ –11 EMX-1Cre:PGC-1 $\alpha^{fl/fl}$. Hippocampus: $n = 9$ –10 EMX-1Cre:PGC-1 $\alpha^{+/+}$, $n = 14$ EMX-1Cre:PGC-1 $\alpha^{+/fl}$, $n = 11$ EMX-1Cre:PGC-1 $\alpha^{fl/fl}$. (G) Representative western blot gels of neocortical and hippocampal homogenate for *Syt2* and (H) quantification of pixel density. $n = 7$ –8 mice/genotype. (I) Representative images of *Syt2*-immunoreactivity in dentate (green, arrows) and quantification. $n = 2$ –6 images/mouse, 3 mice/genotype. The location of higher magnification images is indicated by white box. Representative images per genotype are presented here. Age-related compensatory regulation of PGC-1 α -responsive transcripts are seen in conditional knockouts in neocortex (H) and hippocampus (I). $n = 9$ –13 animals/genotype. * $p < 0.05$; ** $p < 0.01$; *** $p < 0.001$, % $p < 0.0001$; Data are presented as median \pm interquartile range. (For interpretation of the references to colour in this figure legend, the reader is referred to the web version of this article.)

expressed as fold to the respective age control. Transcript levels in the EMX-1Cre:PGC-1 $\alpha^{fl/fl}$ regions were then compared across ages with the *a priori* hypothesis that they would be further decreased, as some populations require PGC-1 α at advanced age to maintain transcriptional homeostasis (McMeekin et al., 2018).

In the neocortex, four genes were statistically significantly higher in EMX-1Cre:PGC-1 $\alpha^{fl/fl}$ mice at one year of age compared to six months (with a one-tailed Mann Whitney): PGC-1 α ($U_{10,10} = 10$, $p = 0.0008$), *Syt2* ($U_{10,13} = 14$, $p = 0.0004$), *Nefh* ($U_{11,13} = 42$, $p = 0.047$), and *Nceh1* ($U_{11,13} = 30$, $p = 0.0077$). *Phyh* ($U_{11,13} = 57$, $p = 0.21$) was unchanged (Fig. 2J).

In the hippocampus (Fig. 2K), transcript for PGC-1 α ($U_{10,13} = 9$, $p < 0.0001$), *Inpp5j* ($U_{11,13} = 27$, $p = 0.0044$), *St8sia1* ($U_{11,13} = 39$, $p = 0.032$), and *Phyh* ($U_{10,13} = 22$, $p < 0.0001$) were significantly higher in EMX-1Cre:PGC-1 $\alpha^{fl/fl}$ mice at one year of age compared to 3 months. The remaining transcripts were unchanged with age: *Syt2* ($U_{11,13} = 68$, $p = 0.43$), *Nefh* ($U_{11,13} = 49$, $p = 0.103$), *Nceh1* ($U_{11,13} = 49$, $p = 0.10$), *Ak1* ($U_{11,13} = 45$, $p = 0.067$), *Pdha1* ($U_{11,13} = 46$, $p = 0.075$), *Stac2* ($U_{11,13} = 65$, $p = 0.37$), *Atp5o* ($U_{11,13} = 45$, $p = 0.067$), *Idh3a* ($U_{11,12} = 39$, $p = 0.052$). Higher expression levels of PGC-1 α -dependent transcripts in aged animals could be due to the compensatory upregulation of PGC-1 α and its dependent genes in other neuronal populations within the neocortex and hippocampus. This hypothesis is supported by the age-dependent increase in PGC-1 α in both tissues. It is also possible that other regulatory factors within EMX-1Cre-positive populations compensate for the loss of PGC-1 α .

Loss of PGC-1 α in PNs influences synaptic drive in the neocortex

To determine the functional and behavioral consequences of PGC-1 α deletion in these neurons, we performed electrophysiological and behavioral experiments. Whole-cell voltage-clamp electrophysiology was used to determine if PGC-1 α deletion influenced excitatory drive in the motor neocortex. The resting membrane potential ($t_{30} = 0.31$, $p = 0.76$) and input resistance ($t_{30} = 0.15$, $p = 0.88$) of layer V PNs were not different between genotypes. AP threshold was significantly reduced in the EMX-1Cre:PGC-1 $\alpha^{fl/fl}$ neurons in response to injected current steps ($t_{29} = 2.76$, $p = 0.01$), though spike number upon current injection at both 150 pA ($t_{29} = 1.16$, $p = 0.26$)

and 300 pA ($t_{22} = 1.055$, $p = 0.30$) was unaffected, suggesting the intrinsic excitability of neocortical PNs in the motor neocortex was minimally altered by PGC-1 α deletion (Table 1).

We also examined the effect of PGC-1 α -deletion on the synaptic release properties of neocortical PNs. Miniature EPSCs (mEPSCs) in layer V PNs, isolated using bicuculline and tetrodotoxin, were recorded as a readout of AP-independent neurotransmitter release from PNs. There was a significant increase in amplitude of mEPSCs observed in EMX-1Cre:PGC-1 $\alpha^{fl/fl}$ PNs compared to controls ($D = 0.13$, $p < 0.0001$) with no change in inter-event interval ($D = 0.030$, $p = 0.057$; Fig. 3A). For spontaneous EPSCs (sEPSCs) in layer V PNs, amplitude was significantly increased ($D = 0.17$, $p < 0.0001$) in EMX-1Cre:PGC-1 $\alpha^{fl/fl}$ PNs as well as inter-event interval ($D = 0.020$, $p = 0.16$; Fig. 3B). While a number of factors could contribute to this result, such as changes in postsynaptic receptor expression, it is clear that there is an increase in the excitatory drive of the motor neocortex of EMX-1Cre:PGC-1 $\alpha^{fl/fl}$ mice.

Entorhinal PNs of the perforant pathway exhibit increased excitability onto dentate GCs

To determine if a loss of PGC-1 α from entorhinal layer II PNs affects neurotransmission onto dentate GCs, we evaluated field potential and granule cell intrinsic properties in slice preparations. A stimulating electrode was placed in the middle molecular layer of the dentate gyrus to activate perforant pathway axons from layer II entorhinal neocortex. Field potentials in the middle molecular layer and GC intrinsic properties and EPSCs via whole-cell voltage clamp were simultaneously recorded. There were no differences in input resistance ($t_{14} = 0.17$, $p = 0.87$), AP threshold ($U_{8,8} = 17$, $p = 0.13$), AP amplitude ($U_{8,8} = 28$, $p = 0.72$), AP frequency ($t_{14} = 0.98$, $p = 0.34$) and after-hyperpolarization amplitude ($U_{8,8} = 28$, $p = 0.69$) of dentate GCs between genotypes, indicating no change in intrinsic properties (Table 2).

We next evaluated excitatory drive in the dentate. Representative traces of fEPSPs and EPSCs are shown in Fig. 3C. Fiber volley (FV) amplitude was used as a measure of the number of recruited axons. For the same stimulus intensity, a RM-ANOVA revealed no significant effect of genotype on FV amplitude ($F_{1,14} = 0.71$, $p = 0.41$) and no interaction between genotype and stimulus intensity ($F_{1,38, 19,314} = 0.296$, $p = 0.67$; Fig. 3D). When fEPSPs and EPSCs from

Table 1. Intrinsic properties of cortical pyramidal neurons

Properties	EMX-1Cre; PGC1 $\alpha^{+/+}$			EMX-1Cre; PGC1 $\alpha^{fl/fl}$			p-value
	Mean	Median	n	Mean	Median	n	
Resting membrane potential	-69.03	-68.85	20	-69.43	-68.7	12	0.76
Input resistance	145.9	133.8	20	142.6	117.5	12	0.88
Action potential threshold	-40.96	-41.9	19	-36.13	-34.1	12	0.01*
Spike number (150 pA)	7.053	7	19	5.083	4.5	12	0.26
Spike number (300 pA)	15.07	16	15	12.33	11	9	0.30

n = number of cells.

*p < 0.05.

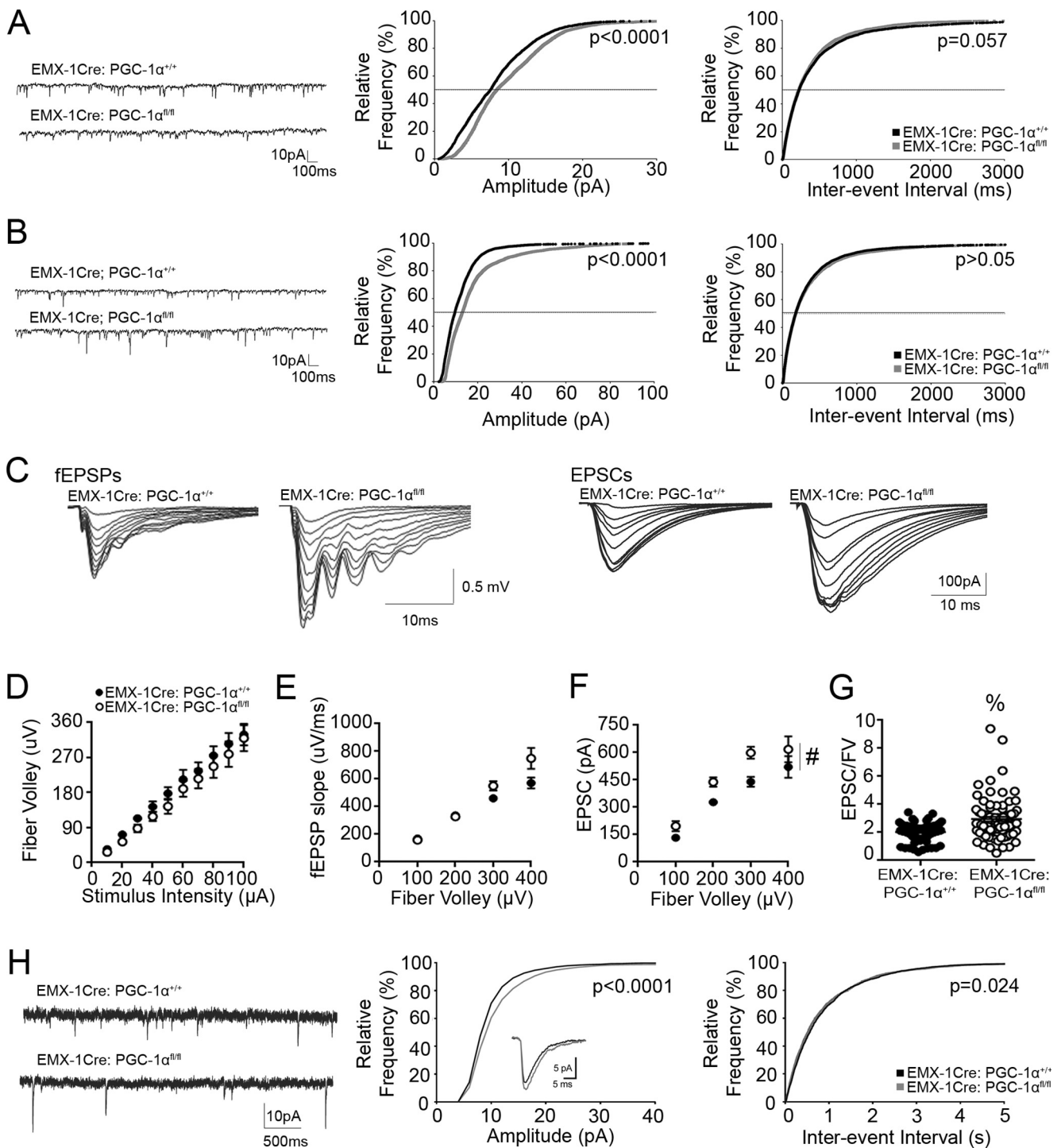


Fig. 3. A loss of PGC-1 α in PNs enhances excitatory transmission. **(A)** Cumulative probability plots of miniature EPSC (mEPSC) amplitude and inter-event interval for layer V pyramidal neurons in 3–5 month-old EMX-1Cre:PGC-1 $\alpha^{+/+}$ and EMX-1Cre:PGC-1 $\alpha^{fl/fl}$ motor neocortex. **(B)** Cumulative probability plots of spontaneous EPSC (sEPSC) amplitude and inter-event interval for layer V pyramidal neurons in the motor cortex. Representative traces for both miniature and spontaneous events are shown in A and B, respectively. Kolmogorov–Smirnov p values are indicated on graphs. mEPSCs, $n = 8–10$ cells/genotype; sEPSCs $n = 10–14$ cells/genotype. **(C)** Representative traces for fEPSPs and EPSCs. Traces represent the average of 10 episodes (10 stim intensities are shown). **(D)** Fiber volley (FV) amplitude in EMX-1Cre:PGC-1 $\alpha^{fl/fl}$ PN projections. **(E)** fEPSP slope at a given FV amplitude in the EMX-1Cre:PGC-1 $\alpha^{fl/fl}$ dentate. **(F)** EPSC amplitude normalized to synaptic transmission of entorhinal PNs onto GCs. **(G)** The ratio of EPSC to FV. **(H)** Representative traces for sEPSC and distribution data of sEPSC amplitude and inter-event interval are shown. * $p < 0.05$; # $p < 0.01$; % $p < 0.0001$, $n = 8$ cells/genotype. Data are presented as mean \pm SEM or median \pm interquartile range.

individual GCs were binned by FV amplitude to normalize for the number of activated presynaptic fibers, there was an increase in synaptic strength. There was a significant

interaction between genotype and stimulus intensity ($F_{2,33, 37,334} = 5.42$, $p = 0.006$; RM-ANOVA) on fEPSP slope; however, post hoc analyses did not reveal

Table 2. Intrinsic properties of dentate granule cells

Properties	EMX-1Cre; PGC1 α ^{+/+}			EMX-1Cre; PGC1 α ^{fl/fl}			p -value
	Mean	Median	n	Mean	Median	n	
Input resistance	329.1	307.3	8	323.2	309.8	8	0.87
Action potential threshold	-41.36	-41.31	8	-44.04	-44.99	8	0.13
Action potential amplitude	80.2	80.87	8	82.93	86.7	8	0.72
Action potential frequency	9.06	8.75	8	10.47	10	8	0.34
Afterhyperpolarization amplitude	-12.49	-12.17	8	-11.79	-11.66	8	0.69

n = number of cells.

significant differences (Fig. 3E). Further, RM-ANOVA revealed a significant effect of genotype on EPSC amplitude for a given FV intensity ($F_{1,13} = 12.23$, $p = 0.004$). There was no interaction between genotype and FV ($F_{1,92, 24.89} = 2.32$, $p = 0.12$; Fig. 3F). Further, there was an overall increase in the EPSC/FV ratio in the EMX-1Cre:PGC-1 α ^{fl/fl} dentate ($U_{77,78} = 1665$, $p < 0.0001$) compared to control (Fig. 3G). No differences were observed in paired pulse ratio, suggesting no change in presynaptic release of neurotransmitter ($t_{137} = 1.23$, $p = 0.22$). sEPSCs were measured in GCs; Kolmogorov-Smirnov test revealed a significant increase in both amplitude ($D = 0.1142$, $p < 0.0001$) and frequency ($D = 0.041$, $p = 0.024$) of sEPSCs (Fig. 3H). It is likely that the increase in population spikes (seen in Fig. 3C) results from the increase excitatory synaptic drive (i.e. increase in the amplitude of EPSPs, EPSCs and sEPSCs) since we did not detect differences in basic measures of GC intrinsic excitability. Overall, there is an increase in excitatory drive of cortical projection neurons onto dentate GCs independent of release probability.

Loss of PGC-1 α in PNs causes increased intrinsic excitability in CA1

Firing properties of CA1 PNs were next measured to determine if a loss of PGC-1 α influenced intrinsic excitability in CA1. The following intrinsic properties were unchanged in CA1 PNs: resting membrane potential ($t_{20} = 0$, $p > 0.99$), input resistance ($t_{20} = 1.14$, $p = 0.27$), action potential amplitude ($t_{19} = 1.07$, $p = 0.30$) and half-width ($t_{19} = 1.10$, $p = 0.28$), latency to initial spike ($t_{19} = 1.31$, $p = 0.21$), rheobase ($U_{10,11} = 28.5$, $p = 0.06$), afterhyperpolarization amplitude ($t_{17} = 0.38$, $p = 0.71$), maximum spike number ($U_{10,11} = 33$, $p = 0.13$), accommodation ($t_{19} = 0.76$, $p = 0.46$) and adaptation at 500 pA ($t_{19} = 1.35$, $p = 0.19$), afterdepolarization amplitude ($t_{16} = 1.54$, $p = 0.14$). However, RM-ANOVA revealed a significant main effect of genotype on initial firing frequency ($F_{1,16} = 7.40$, $p = 0.015$); posthoc analysis revealed an increase in firing frequency in CA1 PNs of EMX-1Cre; PGC-1 α ^{fl/fl} mice compared to controls at 200pA ($p = 0.023$ and 250pA ($p = 0.012$). There was no interaction between genotype and current step ($F_{4,412,70,598} = 1.81$, $p = 0.13$; Fig. 4A). These mice also exhibited a reduced spiking threshold ($t_{19} = 2.09$, $p = 0.049$) (Fig. 4B), and an increased maximum frequency of firing ($U_{10,11} = 13$, $p = 0.0019$)

(Fig. 4C). Additionally, a two-sided Fisher's Exact test indicated that neurons lacking PGC-1 α were more likely to exhibit a burst firing phenotype (82%) compared to control (20%) upon 250 pA current injection ($p = 0.009$; Fig. 4D). Together, these results show that CA1 PNs exhibit enhanced intrinsic excitability in slices from EMX-1Cre; PGC-1 α ^{fl/fl} mice, resulting in increased AP firing (Table 3).

Effects on axon excitability in CA1 are pathway specific

CA1 PNs receive excitatory input from hippocampus via Schaffer Collateral (SC) axons from CA3 PNs, and from layer III of entorhinal neocortex via temporammonic (TA) pathway (perforant pathway) axons. Recording and extracellular stimulating electrodes were placed in *s. radiatum* of CA1 to activate SC axons, and in *s. lacunosum moleculare* of CA1 to activate TA pathway axons. The paired-pulse ratio (PPR) was calculated for both SC synapses and TA synapses (Fig. 4E, H). A significant interaction between genotype and paired-pulse interval was found for SC synapses ($F_{2,709,32,506} = 5.4$, $p = 0.005$); posthoc analysis showed that slices lacking PGC-1 α have a significantly higher PPR at an interval of 50 ms compared to control ($p = 0.01$). On the contrary, there was no effect for genotype ($F_{1,12} = 0.008$, $p = 0.929$) or interaction between genotype and paired-pulse interval for CA1 PNs ($F_{2,183, 26,193} = 2.72$, $p = 0.08$).

FVs in the SC and TA pathways were then measured with increasing stimulus intensities to determine if a loss of PGC-1 α changes axon excitability. There was no effect documented for genotype ($F_{1,12} = 3.225$, $p = 0.098$) or an interaction between genotype and stimulus intensity ($F_{1,679,20,151} = 2.957$, $p = 0.082$) for SC fiber volleys, though differences do approach significance. Interestingly, in the TA pathway, there is an enhancement of fiber volleys in response to increasing stimulation in the EMX-1Cre; PGC-1 α ^{fl/fl} slices compared to control ($F_{1,8} = 17.554$, $p = 0.003$). There was also a significant interaction between genotype and stimulus ($F_{2,306,18,448} = 9.199$, $p = 0.001$) with post hoc analysis revealing a significant difference between 25 μ A, 50 μ A and 75–125 μ A ($p < 0.01$; Fig. 4I). No differences between genotype were detected in the input/output curves (fEPSP slope vs. fiber volley) for either the SC ($F_{1,11} = 0.749$, $p = 0.405$), nor was there a significant interaction ($F_{1,463, 16,089} = 0.255$, $p = 0.709$). There was also no

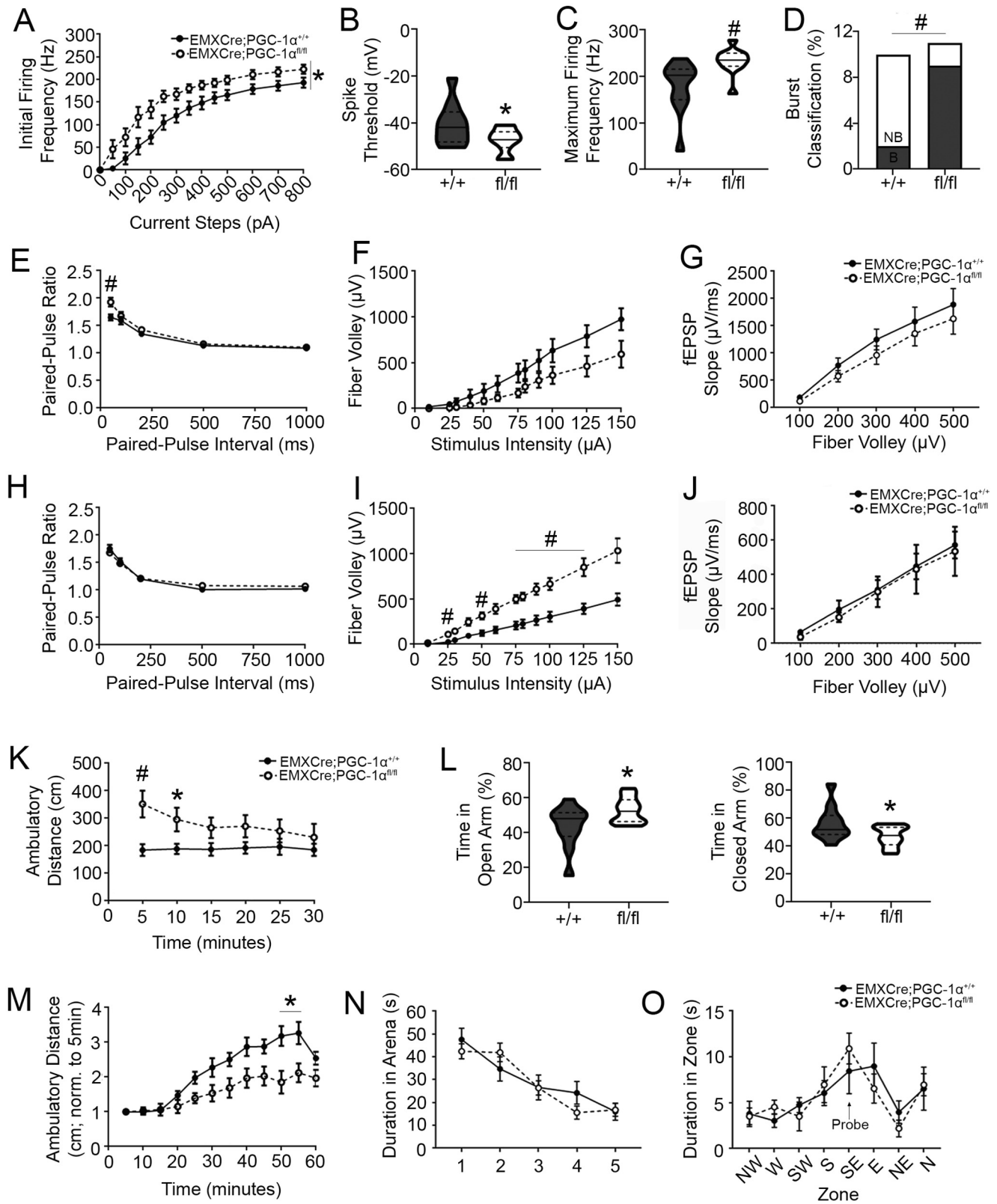


Fig. 4. Excitability in the TA and SC pathways is differentially affected by a loss of PGC-1 α . Intrinsic properties of CA1 PNs are as follows: **(A)** initial firing frequency, **(B)** spike threshold **(C)** max firing frequency, **(D)** burst firing classification. SC pathway properties are as follows: **(E)** paired-pulse ratio (PPR) **(F)** fiber volley (FV) and **(G)** fEPSP slope. TA pathway properties are as follows: **(H)** PPR, **(I)** FV, and **(J)** fEPSP slope. For electrophysiological experiments, intrinsic firing ($n = 9-11$ cells/genotype); field recordings ($n = 5-8$ cells/genotype). At 6–8 months, conditional knockout mice were tested in **(K)** open field ($n = 6-8$ /genotype), **(L)** zero maze ($n = 11, 12$ /genotype) and **(M)** in open field in response to MK-801 ($n = 6, 9$ /genotype) **(N, O)** Spatial memory was assessed using water maze ($n = 6-11$ /genotype). * $p < 0.05$; # $p < 0.01$; \$ $p < 0.001$; % $p < 0.0001$. Data are presented as mean \pm SEM or median \pm interquartile range.

Table 3. Intrinsic properties of CA1 pyramidal neurons

Properties	EMX-1Cre; PGC1 α ^{+/+}			EMX-1Cre; PGC1 α ^{fl/fl}			p-value
	Mean	Median	n	Mean	Median	n	
Resting membrane potential	−69.64	−72	11	−69.64	−72	11	> 0.99
Input resistance	98.18	95	11	87.82	85	11	0.27
Rheobase	152.5	125	10	79.55	75	11	0.06
Spike threshold	−40.54	−41.94	10	−47.16	−47.1	11	0.049
Action potential amplitude	63.26	67.29	10	71.79	75.99	11	0.30
Action potential half-width	1.41	1.3	10	1.23	1.2	11	0.28
Latency to initial spike	171.8	159.5	10	102.5	61	11	0.21
Afterhyperpolarization amplitude	−3.37	−2.82	10	−2.99	−2.49	9	0.71
Maximum spike number	26.23	25.17	10	30.6	30.75	11	0.13
Maximum firing frequency	177.8	202.7	10	233	235.3	11	0.0019*
Accommodation	7.1	6.38	10	5.97	5.79	11	0.46
Adaptation	0.95	0.96	10	0.84	0.83	11	0.19
Afterdepolarization amplitude	9.18	11.09	10	13.53	13.07	8	0.14

n = number of cells.

*p < 0.05.

genotypic effect ($F_{1,11} = 0.093$, $p = 0.766$) or interaction ($F_{1,371,15,084} = 0.035$, $p = 0.916$) in the TA pathway (Fig. 4G, J). These data show enhanced axon excitability largely in the TA pathway and minimal effects on the SC pathway.

Mice lacking PGC-1 α in neocortical and hippocampal pyramidal neurons exhibit hyperactivity in response to a novel environment

PGC-1 α null and neuron-specific knockout mice exhibit severe motor deficits (Lin et al., 2004; Lucas et al., 2012, 2014b). To determine the extent of forebrain PN contribution to these deficits, motor function of 3–5 month-old EMX-1Cre:PGC-1 α ^{fl/fl} mice and controls was assessed using rotarod and open field, both of which revealed significant motor dysfunction in the null mouse (Lucas et al., 2012, 2014b). Upon observation, EMX-1Cre:PGC-1 α ^{fl/fl} mice did not display the tremor or hindlimb clasp seen in PGC-1 α null mice. RM-ANOVA for rotarod revealed no effect of genotype ($F_{1,13} = 0.61$, $p = 0.45$) or interaction between genotype and rotations per minute ($F_{1,34,17.4} = 0.52$, $p = 0.53$), indicating EMX-1Cre:PGC-1 α ^{fl/fl} mice exhibit no overt deficits in coordination. In open field, RM-ANOVA revealed a significant interaction between genotype and time ($F_{4,1,61.2} = 2.71$, $p = 0.037$) for ambulatory distance. Posthoc analysis determined this hyperactivity was significant during the first 5-min period of the 30-min test session ($p = 0.008$) and a trend at 10 min ($p = 0.031$), after which ambulation normalized to that of control (Fig. 4K). Of note, EMX-1Cre:PGC-1 α ^{fl/fl} mice exhibited a significantly increased ambulatory time ($t_{15} = 2.35$, $p = 0.033$) and ambulatory distance in the central zone of the open field ($t_{15} = 2.33$, $p = 0.03$) with no differences in ambulatory time ($t_{15} = 1.48$, $p = 0.16$) or distance in the periphery of the open field between genotypes ($t_{15} = 1.70$, $p = 0.11$). Assessment of activity across all control groups (wildtype, EMX-1Cre:PGC-1 α ^{+/+} and WT; PGC-1 α ^{fl/fl} genotypes; $n = 4$ –5/genotype) showed no main effect of genotype on ambulatory activity ($F_{2,11} = 0.055$,

$p = 0.946$), indicating that the floxed allele alone was not responsible for the ambulatory hyperactivity. These data show that hyperactivity was in response to a novel environment and not indicative of motor impairment or an anxiety-like phenotype.

In order to more adequately assess anxiety-like behavior, mice were tested in the zero maze, in which anxiety-like behavior is indicated by increased time spent in the walled segments of the maze relative to those that are exposed. EMX-1Cre:PGC-1 α ^{+/+} mice spent significantly more time in the closed segment of the zero maze compared to EMX-1Cre:PGC-1 α ^{fl/fl} mice and vice versa for the open arm ($t_{21} = 2.24$, $p = 0.036$). Though data may indicate that conditional knockouts at 6–8 months of age do not exhibit the inherent anxiety-like phenotype of EMX-1Cre:PGC-1 α ^{+/+} mice (Fig. 4L), it is also possible that this represents an increased exploratory drive.

Mice lacking PGC-1 α in PNs show an overall increased excitatory drive. To test the effects of blocking NMDA receptors *in vivo* on ambulatory activity, we administered 0.2 mg/kg MK-801 intraperitoneally and immediately placed animals into open field (Fig. 4M). Because cell-specific knockouts exhibit an initial increase in exploratory behavior, ambulatory distance was normalized for each animal to that the first five min of testing. A RM-ANOVA revealed a significant main effect of genotype ($F_{1,14} = 7.14$, $p = 0.02$) and an interaction between time and genotype ($F_{2,13,29.86} = 4.87$, $p = 0.013$). Posthoc analysis identified a significant reduction in ambulation for conditional knockouts compared to littermate controls at 50 and 55 min ($p = 0.013$ and $p = 0.018$, respectively).

To investigate the effects of forebrain PGC-1 α deletion on spatial working memory, animals were tested in water maze at 6–8 months of age. A RM-ANOVA revealed no significant difference between genotype over the five-day session ($F_{1,15} = 0.11$, $p = 0.74$; Fig. 4N). Further, a RM-ANOVA revealed a significant main effect of time ($F_{4,60} = 24.59$, $p < 0.0001$), and posthoc analyses demonstrated

significant differences between day 1 and day 5 latencies for both EMX-1Cre:PGC-1 $\alpha^{fl/fl}$ and control animals ($p < 0.0001$) indicating both genotypes learned the task. No difference between genotypes in the probe trial ($F_{1,15} = 0.10$, $p = 0.75$) were seen, demonstrating that EMX-1Cre: PGC-1 $\alpha^{fl/fl}$ mice still retain spatial learning abilities (Fig. 4O).

To test if ambulatory activity was affected with age, animals were tested at 1 year. RM-ANOVA indicated no significant difference between genotypes for ambulatory distance in open field ($F_{1,26} = 0.024$, $p = 0.88$), nor was there an interaction between genotype and time ($F_{2,34,60,93} = 0.75$, $p = 0.50$). Additionally, there was no genotypic difference in water maze ($F_{1,20} = 0.078$, $p = 0.78$). Of note, there was a main effect of time on water maze ($F_{4,80} = 16.99$, $p < 0.0001$) with significant posthoc differences between day 1 and day 5 for both EMX-1Cre:PGC-1 $\alpha^{+/+}$ ($p = 0.0002$) and EMX-1Cre:PGC-1 $\alpha^{fl/fl}$ ($p = 0.0002$) mice suggesting both genotypes

learned over the course of the assay. There was no difference between genotypes for time spent in the zone of the platform ($F_{1,26} = 0.024$, $p = 0.88$) for the probe task further indicating that learning remains intact with age.

A subset of novel PN-enriched, PGC-1 α -dependent transcripts are reduced in the conditional knockout neocortex and hippocampus

Previous transcriptional studies identifying PGC-1 α -dependent transcripts were not conducted with the intent of finding those that were selectively enriched in PNs *in vivo*. Thus, to identify putative novel PN-enriched PGC-1 α -dependent genes, we compared genes upregulated twofold in SH-SY5Y neuroblastoma cells overexpressing PGC-1 α (Lucas et al., 2014a) to transcripts enriched in neocortical excitatory neurons compared to the entire neocortex (Mo et al., 2015) (Fig. 5A, B). To increase our chances of identifying novel PGC-

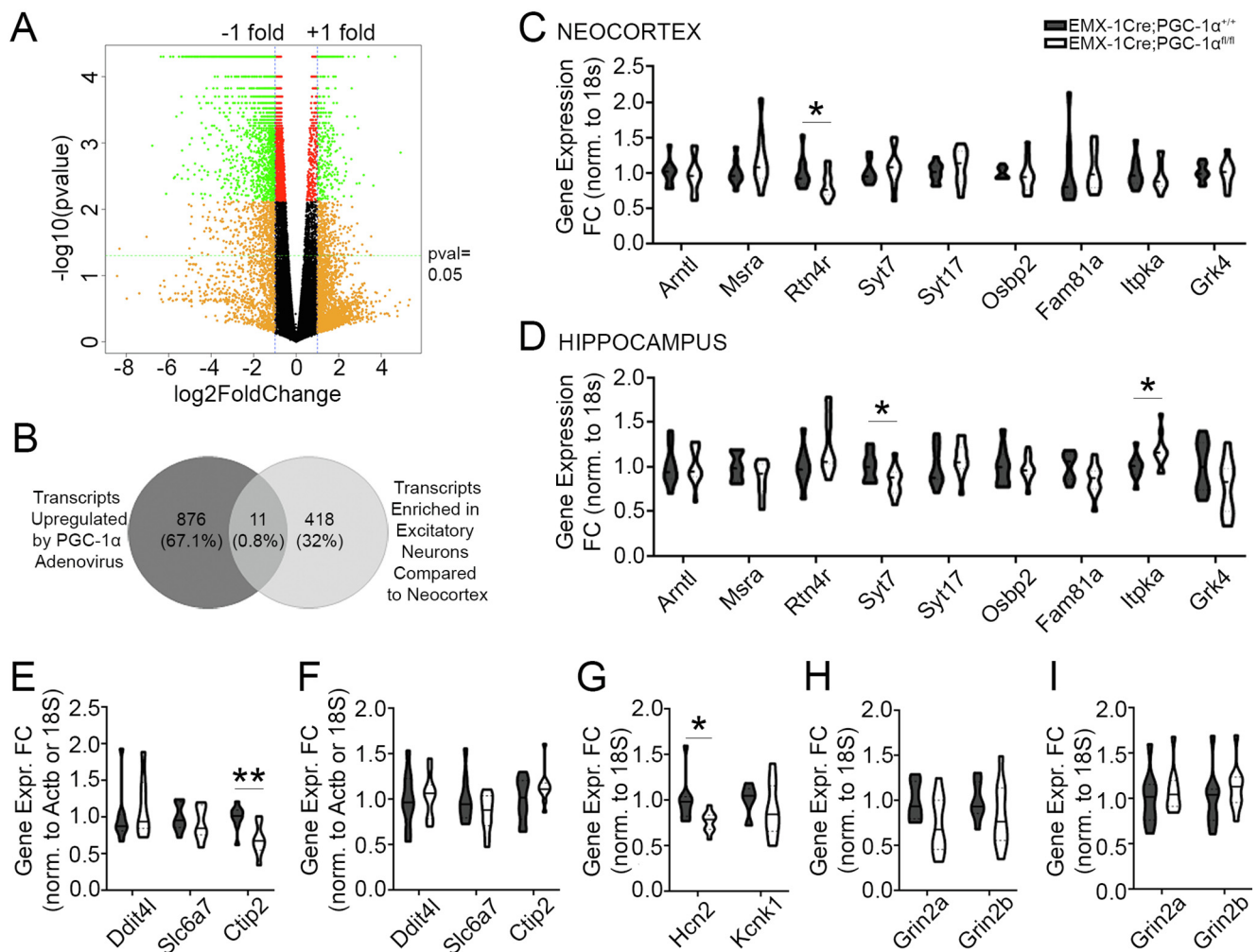


Fig. 5. A subset of PN-enriched PGC-1 α -responsive transcripts is reduced in the conditional knockout neocortex and hippocampus. **(A, B)** Comparison of transcripts upregulated by PGC-1 α adenovirus *in vitro* and transcripts enriched in excitatory neurons relative to neocortical homogenate identified 11 genes as putative PGC-1 α targets in PNs. **(C)** These were measured in the conditional knockout neocortex and **(D)** hippocampus. **(E)** Transcripts labeling cortical layers were assessed in the neocortex and **(F)** hippocampus. **(G)** Transcripts for genes linked to neuronal excitability were measured in the neocortex. **(H)** Grin2a and Grin2b were measured in neocortex and **(I)** hippocampus. $n = 9$ –11/genotype. * $p < 0.05$; ** $p < 0.01$; *** $p < 0.001$; Data are presented as median \pm interquartile range.

1 α -dependent genes that are enriched in PNs and detectable in a neocortical homogenate, we used the dataset from Mo et al. which compared transcripts enriched in neocortical excitatory neurons with respect to transcripts expressed throughout all cell types in neocortical homogenates (Fig. 5). We then compared this list to the list of genes significantly upregulated by PGC-1 α overexpression in neuroblastoma cells (Lucas et al., 2014a). These transcripts included *Arntl*, *Msra*, *Rtn4r*, *Syt7*, *Syt17*, *Osbp2*, *Fam81a*, *Itpka*, and *Grk4* (See Supplemental Table 1 for gene names). Under the *a priori* hypothesis that these transcripts would be reduced with a loss of PGC-1 α , we measured these transcripts in the EMX1Cre; PGC-1 $\alpha^{fl/fl}$ neocortex and hippocampus compared to control at 3–5 months of age. Amongst the transcripts measured, *Rtn4r* ($U_{9,10} = 24$, $p = 0.047$), was significantly reduced in the neocortex (Fig. 5C). The remaining transcripts were unaffected in the conditional knockout neocortex: *Arntl* ($U_{9,10} = 37$, $p = 0.27$), *Msra* ($U_{9,10} = 32$, $p = 0.16$), *Syt7* ($U_{9,10} = 33$, $p = 0.18$), *Syt17* ($U_{9,10} = 0.32$, $p = 0.16$), *Osbp2* ($U_{9,10} = 34$, $p = 0.20$), *Fam81a* ($U_{9,9} = 29$, $p = 0.17$), *Itpka* ($U_{9,10} = 35$, $p = 0.22$), *Grk4* ($U_{9,9} = 38$, $p = 0.43$).

Amongst those measured in the conditional knockout hippocampus (Fig. 5D), transcripts for *Syt7* ($U_{9,11} = 24$, $p = 0.028$) and *Itpka* ($U_{9,11} = 21$, $p = 0.016$) were significantly affected by a loss of PGC-1 α , the former being downregulated and the latter being upregulated. Transcripts for the remaining genes were unchanged: *Arntl* ($U_{9,11} = 46$, $p = 0.41$), *Msra* ($U_{9,11} = 32$, $p = 0.10$), *Rtn4r* ($U_{9,11} = 28$, $p = 0.056$), *Syt17* ($U_{9,11} = 36$, $p = 0.17$), *Osbp2* ($U_{9,11} = 49$, $p = 0.50$), *Fam81a* ($U_{9,11} = 28$, $p = 0.056$), and *Grk4* ($U_{9,11} = 29$, $p = 0.065$).

There was an *a priori* hypothesis that these transcripts would likely be reduced with age. While *Rtn4r* transcript was reduced in neocortex at 3–5 months, there was no difference between genotypes for *Rtn4r* transcript in the neocortex at a year of age ($U_{9,13} = 43$, $p = 0.16$), nor were there differences at a year of age in the hippocampal for transcripts: *Syt7* ($U_{9,13} = 50$, $p = 0.30$), and *Itpka* ($U_{9,13} = 58$, $p = 0.50$). These data suggest that at basal conditions with age, compensation occurs for these transcripts by pathways that do not rely on intrinsic PGC-1 α activity.

To investigate whether PGC-1 α deletion has an effect on specific neocortical layers, we measured transcriptional identifiers of neocortical layers II/III (*Ddit4l*) and IV/V (*Slc6a7*, *Ctip2*). Interestingly, while there was no change in *Ddit4l* ($U_{9,7} = 27$, $p = 0.68$) or *Slc6a7* ($U_{9,7} = 22$, $p = 0.35$), *Ctip2* was significantly reduced in the conditional knockout neocortex compared to control ($U_{9,8} = 9$, $p = 0.0079$) (Fig. 5E). Considering the maintenance of *Slc6a7*, these data suggest that, though *Ctip2* is reduced, cell number of these neocortical layers is seemingly intact. No differences were detected in *Ddit4l* ($U_{9,10} = 38$, $p = 0.60$), *Slc6a7* ($U_{9,10} = 34$, $p = 0.40$) or *Ctip2* ($U_{9,10} = 41$, $p = 0.55$), transcripts enriched in CA1, CA2/3, and CA1/dentate, respectively, in the conditional knockout hippocampus (Fig. 5F).

Considering the increase in excitability in neocortical projections in the conditional knockout, we next measured transcript for two genes involved in excitability that are upregulated by PGC-1 α *in vitro*, hyperpolarization-activated cyclic nucleotide-gated K⁺ 2 (*Hcn2*) and potassium two pore domain channel subfamily K member 1 (*Kcnk1*). No differences were detected in *Kcnk1* transcript between EMX1Cre:PGC-1 $\alpha^{+/+}$ and EMX1Cre:PGC-1 $\alpha^{fl/fl}$ neocortex ($U_{9,10} = 33$, $p = 0.36$) (Fig. 5G). However, there was a significant reduction in transcript for *Hcn2* in the conditional knockout compared to control ($U_{9,10} = 14$, $p = 0.01$) (Fig. 5G).

To test if glutamate receptors were influenced by a loss of PGC-1 α in PNs, we tested transcript for the NMDA receptor subunits *Grin2a* and *Grin2b*. In the neocortex, there were no differences between EMX1Cre:PGC-1 $\alpha^{+/+}$ and EMX1Cre:PGC-1 $\alpha^{fl/fl}$ samples for either *Grin2a* ($U_{9,10} = 26$, $p = 0.13$) and *Grin2b* ($U_{9,10} = 28$, $p = 0.18$; Fig. 5H). There was also no difference between genotypes in the hippocampus for *Grin2a* ($U_{9,11} = 42$, $p = 0.60$) or *Grin2b* ($U_{9,11} = 32$, $p = 0.20$) transcript (Fig. 5I).

PGC-1 α -dependent transcription is largely unaffected in the neocortex and hippocampus of knock-in models for HD

Several studies suggest that reductions in PGC-1 α contribute to HD pathogenesis, as PGC-1 α mRNA expression is reduced in the caudate/striatum from both human post mortem and murine HD models (Cui et al., 2006; Weydt et al., 2006; Chaturvedi et al., 2010). Recent findings from our lab indicate that PGC-1 α deficiency selectively in the most vulnerable neuronal population in HD, MSNs, is not sufficient to cause an HD-like phenotype in mice (McMeekin et al., 2018). Neocortical pathology and cognitive dysfunction are prevalent in HD (Sieradzan and Mann, 2001). Interestingly, deletion of PGC-1 α from excitatory neurons (CAMKII α +) leads to the development of vacuoles throughout the forebrain (Ma et al., 2010). Here, we tested if PGC-1 α and genes downregulated in the cell-specific knockout neocortex and hippocampus showed a similar pattern of regulation in a series of HDQ knockin mice used previously to investigate PGC-1 α -dependent gene expression in the striatum (McMeekin et al. 2018).

The homozygous HDQ knockin line expresses increasing CAG repeat length of the *mhtt* gene on both alleles with no substantial loss of neuron number (Kumar et al., 2016). No significant differences were detected in the neocortex (Fig. 6A) for PGC-1 α ($H_4 = 1.13$, $p = 0.89$), *Syt2* ($H_4 = 1.70$, $p = 0.79$), *Nefh* ($H_4 = 1.75$, $p = 0.78$), *Nceh1* ($H_4 = 1.81$, $p = 0.77$) or *Phyh* ($H_4 = 2.86$, $p = 0.58$). We next measured gene expression for PGC-1 α -dependent genes in the hippocampus from these same animals (Fig. 6B). No significant differences were detected amongst the genotypes for PGC-1 α ($H_4 = 4.59$, $p = 0.33$) and *Syt2* ($H_4 = 2.11$, $p = 0.72$). There were differences across genotypes for *Nefh* ($H_4 = 10.13$, $p = 0.04$), however post hoc analyses revealed no differences compared to wildtype. Amongst

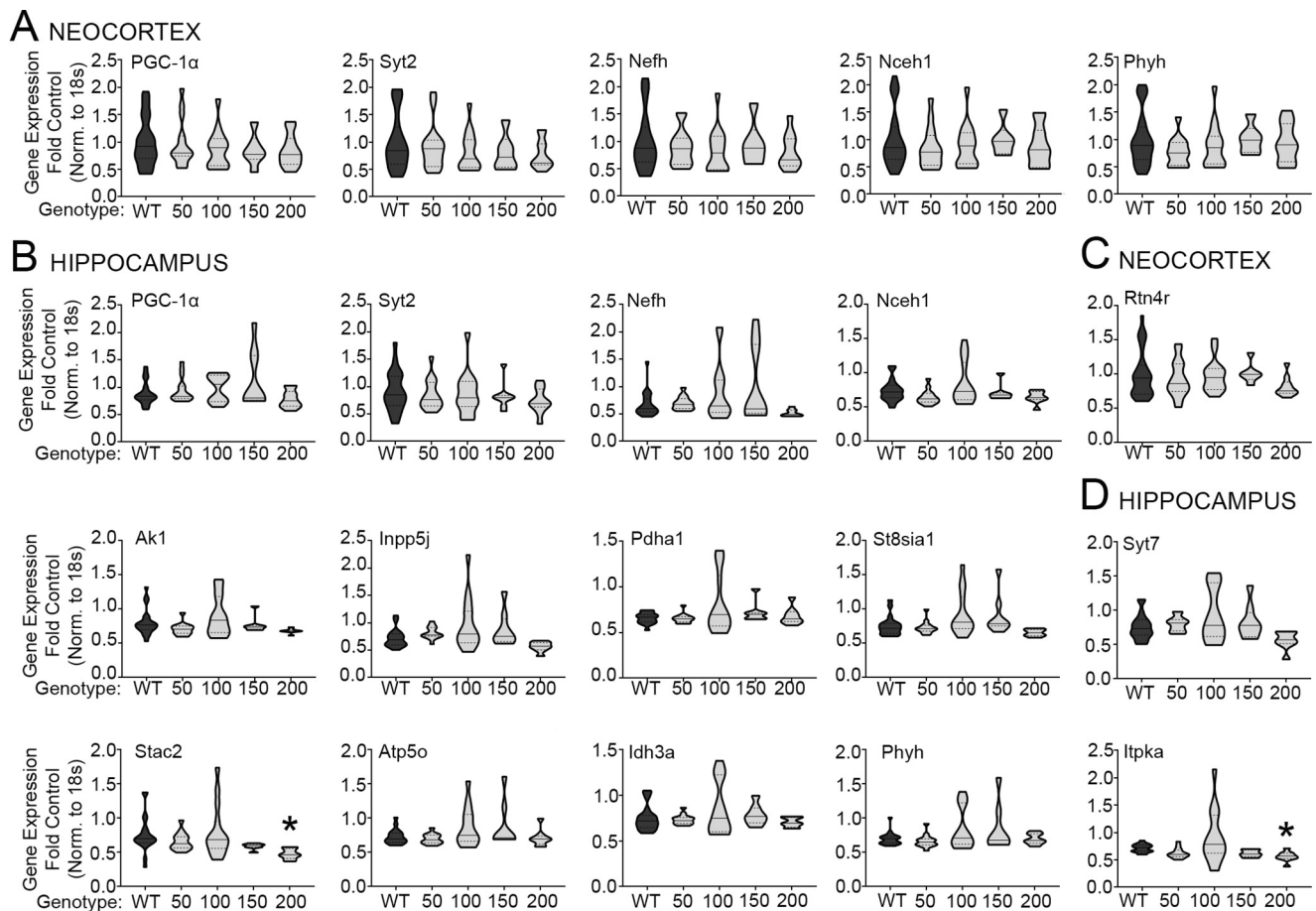


Fig. 6. PGC-1 α -dependent transcription is largely unaffected in the HDQ knock-in model of HD. **(A)** The expression of PGC-1 α and its dependent genes were measured in the neocortex and **(B)** hippocampus of 6 month-old HDQ knock-in mice (homozygous genotypes listed below graphs). **(C)** PGC-1 α -dependent PN-enriched transcripts were also assessed in the HDQ neocortex and **(D)** hippocampus of the HDQ^{200/200} line compared to control. $n = 6$ –29/genotype for neocortex, $n = 7$ –22/genotype for hippocampus. * $p < 0.05$; Data are presented as median \pm interquartile range.

the transcripts not specific to neurons, only *Stac2* transcript was significantly different amongst the groups ($H_4 = 17.78$, $p = 0.0014$); posthoc analysis revealed a significant reduction of *Stac2* transcript in the 200/200 hippocampus compared to WT ($p = 0.0003$; Fig. 6B). Transcripts for the following genes were unchanged: *Nceh1* ($H_4 = 6.73$, $p = 0.15$), *Ak1* ($H_4 = 8.88$, $p = 0.064$), *Pdha1* ($H_4 = 2.72$, $p = 0.61$), *Atp5o* ($H_4 = 4.71$, $p = 0.32$), *ldh3a* ($H_4 = 1.89$, $p = 0.76$), *Phyh* ($H_4 = 2.90$, $p = 0.58$). While significant differences amongst the genotypes were found for *Inpp5j* ($H_4 = 16.83$, $p = 0.0021$) and *St8sia1* ($H_4 = 15.28$, $p = 0.0042$), posthoc revealed no differences compared to wildtype.

We also tested novel, PN-enriched transcripts in the HDQ neocortex and hippocampus that were altered in the EMX-1Cre;PGC-1 $\alpha^{fl/fl}$ knockout brain. There was no change in *Rtn4r* transcript ($H_4 = 5.10$, $p = 0.28$) in the HDQ neocortex (Fig. 6C). Similarly, transcripts that were downregulated in the EMX-1Cre;PGC-1 $\alpha^{fl/fl}$ hippocampus were then measured in the HDQ allelic series (Fig. 6D). Significant differences across genotypes were found for *Itpka* ($H_4 = 18.14$, $p = 0.0012$); posthoc analysis revealed transcript

reductions in the 50/50 ($p = 0.047$) and 200/200 ($p = 0.0042$) genotypes compared to wildtype. Though there significant were differences in transcript across genotypes for *Syt7* ($H_4 = 11.58$, $p = 0.021$), post hoc analysis revealed no differences compared to control. These data show that, in general, genes dependent on PGC-1 α for their normal expression are not affected in the neocortex or hippocampus of the HDQ knockin model mouse. This suggests that PGC-1 α deficiency or dysfunction is not occurring in the neocortex in this model, despite transcriptional changes we (McMeekin et al. 2018) and others have shown in these mice.

DISCUSSION

Several lines of evidence indicate region-specific and cell-type-specific effects on transcription and electrophysiological properties in the absence of PGC-1 α , making it difficult to understand how PGC-1 α deficiency contributes to disease. PGC-1 α null mice exhibit robust motor deficits (Lin et al., 2004; Leone et al., 2005; Lucas et al., 2012, 2014b) that are recapitulated by nervous system-specific deletion (Lucas et al., 2012) but absent when deleted from PV-INs or MSNs

(Lucas et al., 2014a; Bartley et al., 2015; McMeekin et al., 2018). Additionally, reductions in transcripts involved in metabolism (Lin et al., 2004; Cowell et al., 2009; Lucas et al., 2014a), synchronous neurotransmitter release (Syt2, Cplx1) and axonal structure (Nefh) are reduced in the PGC-1 α null neocortex (Lucas et al., 2014a) but differentially regulated in homogenate from cell-specific deletion studies across brain regions (Lucas et al., 2014a; Bartley et al., 2015; McMeekin et al., 2018). Notably, enhanced excitability in the null neocortex (Dougherty et al., 2014a) is not recapitulated by PV-IN-specific deletion (Lucas et al., 2014a). In contrast, the PGC-1 α null hippocampus favors an inhibited state that is recapitulated with PV-IN-specific deletion (Bartley et al., 2015). These data indicate that PGC-1 α is required for normal transcription and function of forebrain PN and PV-INS and that deletion of PGC-1 α in either of these populations alone is not sufficient to generate the phenotype of PGC-1 α null mice.

The absence of PGC-1 α in cortical PNs enhanced intrinsic excitability in the motor neocortex and excitatory drive in the neocortico-hippocampal circuit. These data are in contrast to what we have previously shown in the PGC-1 α null mouse, in which presynaptic release of glutamate onto PV-INS was reduced (Dougherty et al., 2014a). Further, global loss of PGC-1 α in the hippocampus alters the excitatory:inhibitory (E:I) balance to favor enhanced basal inhibition and limited CA1 PN activity (Bartley et al., 2015). Here, a loss of PGC-1 α in PNs favors an excitable state. These differences may reflect contributions of interneuron and/or thalamic abnormalities in the global PGC-1 α knockout and highlight the need to perform cell-type-specific deletion studies to evaluate how cell-autonomous dysfunction influences the circuit. It is interesting to speculate that enhanced excitability in the cortico-hippocampal circuit the EMX-1Cre mouse would consequently increase activity of inhibitory interneurons. While the E:I balance in this line appears to favor an excitable state, it is possible that inhibition in this circuit creates a condition whereby PNs lacking PGC-1 α adjust accordingly with lower activation thresholds and enhanced burst firing (Desai et al., 1999). Though not reported here for cortical PNs, an increased number of CA1 PNs exhibit a burst firing profile. Along with fully investigating the E:I balance in these animals, changes in persistent sodium currents and calcium-gated potassium currents are thought to be regulators of burst firing (Azouz et al., 1996; Williams and Stuart, 1999) as well as changes in intrinsic properties seen here. Further studies are warranted to parse out the contribution of these and other mechanisms to the changes in neurotransmission.

There are several contributors to the enhanced excitability seen in the cortico-hippocampal circuit, one being regulation of region-specific transcription. Our data suggest hippocampal PNs may be more reliant on PGC-1 α to meet metabolic demand as transcript levels of these genes are more robustly reduced in this region compared to neocortex. Knockdown of PGC-1 α in hippocampal neurons *in vitro* reduces the number of dendritic mitochondria and ATP production (Cheng

et al., 2012), and the mitochondrial transcript *Cox1* is reduced in the hippocampus of mice lacking PGC-1 α selectively in these neurons. While the effects of PN-specific loss of PGC-1 α on mitochondrial number is unknown, our data suggest that these mitochondria are impaired. As such, their capacity for generating reactive oxygen species may be elevated, and their ability to buffer calcium subsequently compromised. These two factors could potentially contribute to an excitable state in both the neocortex and hippocampus, and provide a plausible mechanism for the differences in excitability that we see in conditional knockouts. Additionally, while Syt2 transcript is reduced in neocortex and hippocampus, limited changes in presynaptic properties are seen in either region in EMX-1Cre;PGC-1 α ^{fl/fl} mice. While it is possible asynchronous neurotransmitter release would be evident with more stringent protocols (Lucas et al., 2014a), it is equally possible that Syt1 compensates for Syt2 in these mice.

There are several factors that contribute to the discrepancy in gene expression regulated by PGC-1 α amongst the null and cell-specific knockout mice. As PGC-1 α is a transcriptional coactivator, its effects within a cell are dependent on the milieu of transcription factors present. Thus, the distinct profile of transcription machinery interacting with PGC-1 α for a PV-IN versus a PN would in turn directly affect what transcripts are responsive to changes in the expression of that coactivator. The expression of cell-type-specific PGC-1 α -interacting transcription factors across regions and cell-types remains to be investigated. To further complicate understanding of cell-type specific PGC-1 α -dependent gene regulation are the multiple splice variants of PGC-1 α that have been identified (Soyal et al., 2012; Martínez-Redondo et al., 2015). Previous studies indicate that genes involved in neurotransmission and metabolism are reduced in the neocortex of mice lacking PGC-1 α ; however, metabolic transcripts are expressed normally in the neocortex of animals retaining the N-terminal domain (Lucas et al., 2014a), indicating that the full length PGC-1 α variant is required for regulation of neuron-enriched genes. Identifying cell-type-specific PGC-1 α -interacting factors will be key in determining its normal function and how its loss in distinct cell populations contributes to varied phenotypes.

Though the hallmark pathology of HD is striatal degeneration, substantial evidence implicates vulnerability of neocortical pyramidal neurons. Neocortical pathology has been documented in HD patients (Sotrel et al., 1991; Rosas et al., 2008), and neocortical cell loss has been reported in postmortem human HD (Cudkovic and Kowall, 1990; Hedreen et al., 1991; Heinsen et al., 1994; Rajkowska et al., 1998) and a model of juvenile HD (Giampà et al., 2010). In fact, neocortical neuron inclusions of mHtt are shown to predict behavioral and electrophysiological abnormalities in a transgenic HD mouse line (HD46, HD100) with altered MSN responsivity to excitatory stimulation (Laforet et al., 2001). Several studies link reductions in PGC-1 α or its downstream targets to HD pathology in human postmortem samples and murine models (Cui et al., 2006; Weydt et al., 2006;

Chaturvedi et al., 2010). Recently, our lab reported that PGC-1 α mRNA expression is not reduced in the striatum of heterozygous or homozygous knockin mHtt models, and that PGC-1 α deficiency solely in MSNs is not sufficient to cause HD-like behaviors or striatal atrophy (McMeekin et al., 2018). Using neocortical and hippocampal tissue from the homozygous knockin lines, we demonstrate here that expression of PGC-1 α and most of its dependent genes are unchanged. Since data demonstrate that conditional deletion from CAMKII-positive populations leads to neocortical and striatal vacuoles (Ma et al., 2010), we cannot rule out the possibility that loss of PGC-1 α in both MSNs and neocortical afferents would lead to an HD-like phenotype. Even so, the lack of mHtt-associated effects on PGC-1 α -dependent genes in neocortex suggest the mHtt does not interfere with cell-autonomous PGC-1 α -dependent transcriptional programs. Additionally, we have demonstrated that selective induction of mHtt expression in PV-INs does not change expression of PGC-1 α or the most robust PGC-1 α -dependent gene, Pvalb (Dougherty et al., 2014b).

In summary, we have found that PGC-1 α regulates gene expression to a lesser extent in PNs than in PV-INs of the forebrain and that deletion of PGC-1 α in one neuron type is not sufficient to recapitulate the effects of whole body knockdown. These results should be taken into account when interpreting how PGC-1 α modulation influences disease etiology and progression. Also, these data suggest that PGC-1 α is not central to transcriptional dysregulation in HD models, raising questions about its potential as a therapeutic target. However, as a number of psychiatric and neurological disorders involve dysregulation of neuronal excitability, mitochondrial function, and neurotransmitter release, it could be useful to identify which PGC-1 α -associated factors are responsible for directing PGC-1 α -dependent gene expression programs in a cell-type-specific manner. Future experiments are required to identify these factors *in vivo*.

CONFLICTS OF INTEREST

The authors have no conflicts of interest to disclose.

ACKNOWLEDGEMENTS

This work was supported by the National Institute of Mental Health (5K01MH077955-05, RMC; R01MH098534, LED; 5R01NS064025, LOW) and the National Institute of Neurological Disorders and Stroke (5R01NS070009-05, 5R01NS101958-02, RMC). Many thanks are due to the UAB Center for Neurodegeneration and Experimental Therapeutics for access to the confocal microscope. Behavioral studies were performed with equipment and training provided by the Evelyn F. McKnight UAB Neurobiology Behavior Core and UAB Neuroscience Behavioral Assessment Core (NIH Grant P30NS047466).

REFERENCES

- Azouz R, Jensen MS, Yaari Y (1996) Ionic basis of spike afterdepolarization and burst generation in adult rat hippocampal CA1 pyramidal cells. *J Physiol (Lond)* 492:211–223.
- Bartley AF, Lucas EK, Brady LJ, Li Q, Hablitz JJ, Cowell RM, Dobrunz LE (2015) Interneuron transcriptional dysregulation causes frequency-dependent alterations in the balance of inhibition and excitation in hippocampus. *J Neurosci* 35:15276–15290.
- Bayer H, Lang K, Buck E, Higelin J, Barteczko L, Pasquarelli N, Sprissler J, Lucas T, Holzmann K, Demestre M, Lindenberg KS, Danzer KM, Boeckers T, Ludolph AC, Dupuis L, Weydt P, Witting A (2017) ALS-causing mutations differentially affect PGC-1 α expression and function in the brain vs. peripheral tissues. *Neurobiol Dis* 97:36–45.
- Chaturvedi RK, Calingasan NY, Yang L, Hennessey T, Johri A, Beal MF (2010) Impairment of PGC-1 α expression, neuropathology and hepatic steatosis in a transgenic mouse model of Huntington's disease following chronic energy deprivation. *Hum Mol Genet* 19:3190–3205.
- Cheng A, Wan R, Yang J-L, Kamimura N, Son TG, Ouyang X, Luo Y, Okun E, Mattson MP (2012) Involvement of PGC-1 α in the formation and maintenance of neuronal dendritic spines. *Nat Commun* 3:1250.
- Clark J, Reddy S, Zheng K, Betensky RA, Simon DK (2011) Association of PGC-1 α polymorphisms with age of onset and risk of Parkinson's disease. *BMC Med Genet* 12:69.
- Cowell RM, Blake KR, Russell JW (2007) Localization of the transcriptional coactivator PGC-1 α to GABAergic neurons during maturation of the rat brain. *J Comp Neurol* 502:1–18.
- Cowell RM, Talati P, Blake KR, Meador-Woodruff JH, Russell JW (2009) Identification of novel targets for PGC-1 α and histone deacetylase inhibitors in neuroblastoma cells. *Biochem Biophys Res Commun* 379:578–582.
- Cudkovic M, Kowall NW (1990) Degeneration of pyramidal projection neurons in Huntington's disease cortex. *Ann Neurol* 27:200–204.
- Cui L, Jeong H, Brovecki F, Parkhurst CN, Tanese N, Krainc D (2006) Transcriptional repression of PGC-1 α by mutant huntingtin leads to mitochondrial dysfunction and neurodegeneration. *Cell* 127:59–69.
- Dervishi I, Gozutok O, Murman K, Gautam M, Heller D, Bigio E, Ozdinler PH (2018) Protein-protein interactions reveal key canonical pathways, upstream regulators, interactome domains, and novel targets in ALS. *Sci Rep* 8:14732.
- Desai NS, Rutherford LC, Turrigiano GG (1999) Plasticity in the intrinsic excitability of cortical pyramidal neurons. *Nat Neurosci* 2:515–520.
- Dougherty SE, Bartley AF, Lucas EK, Hablitz JJ, Dobrunz LE, Cowell RM (2014a) Mice lacking the transcriptional coactivator PGC-1 α exhibit alterations in inhibitory synaptic transmission in the motor cortex. *Neuroscience* 271:137–148.
- Dougherty SE, Hollimon JJ, McMeekin LJ, Bohannon AS, West AB, Lesort M, Hablitz JJ, Cowell RM (2014b) Hyperactivity and cortical disinhibition in mice with restricted expression of mutant huntingtin to parvalbumin-positive cells. *Neurobiol Dis* 62:160–171.
- Ebrahim AS, Ko L-W, Yen S-H (2010) Reduced expression of peroxisome-proliferator activated receptor gamma coactivator-1 α enhances alpha-synuclein oligomerization and down regulates AKT/GSK3 β signaling pathway in human neuronal cells that inducibly express alpha-synuclein. *Neurosci Lett* 473:120–125.
- Eschbach J, Schwalenstöcker B, Soyal SM, Bayer H, Wiesner D, Akimoto C, Nilsson A-C, Birve A, Meyer T, Dupuis L, Danzer KM, Andersen PM, Witting A, Ludolph AC, Patsch W, Weydt P (2013) PGC-1 α is a male-specific disease modifier of human and experimental amyotrophic lateral sclerosis. *Hum Mol Genet* 22:3477–3484.

- Eschbach J, von Einem B, Müller K, Bayer H, Scheffold A, Morrison BE, Rudolph KL, Thal DR, Witting A, Weydt P, Otto M, Fauler M, Liss B, McLean PJ, Spada ARL, Ludolph AC, Weishaupt JH, Danzer KM (2015) Mutual exacerbation of peroxisome proliferator-activated receptor γ coactivator 1 α deregulation and α -synuclein oligomerization. *Ann Neurol* 77:15–32.
- Fox MA, Sanes JR (2007) Synaptotagmin I and II are present in distinct subsets of central synapses. *J Comp Neurol* 503:280–296.
- Giampà C, Laurenti D, Anzilotti S, Bernardi G, Menniti FS, Fusco FR (2010) Inhibition of the striatal specific phosphodiesterase PDE10A ameliorates striatal and cortical pathology in R6/2 mouse model of Huntington's disease. *PLoS One* 5 e13417.
- Gong B, Pan Y, Vempati P, Zhao W, Knable L, Ho L, Wang J, Sastre M, Ono K, Sauve AA, Pasinetti GM (2013) Nicotinamide riboside restores cognition through an upregulation of proliferator-activated receptor- γ coactivator 1 α regulated β -secretase 1 degradation and mitochondrial gene expression in Alzheimer's mouse models. *Neurobiol Aging* 34:1581–1588.
- Gorski JA, Talley T, Qiu M, Puelles L, Rubenstein JLR, Jones KR (2002) Cortical excitatory neurons and glia, but not GABAergic neurons, are produced in the Emx1-expressing lineage. *J Neurosci* 22:6309–6314.
- Hedreen JC, Peyser CE, Folstein SE, Ross CA (1991) Neuronal loss in layers V and VI of cerebral cortex in Huntington's disease. *Neurosci Lett* 133:257–261.
- Heinsen H, Strik M, Bauer M, Luther K, Ulmar G, Gangnus D, Jungkunz G, Eisenmenger W, Götz M (1994) Cortical and striatal neurone number in Huntington's disease. *Acta Neuropathol* 88:320–333.
- Jiang H, Kang S-U, Zhang S, Karuppagounder S, Xu J, Lee Y-K, Kang B-G, Lee Y, Zhang J, Pletnikova O, Troncoso JC, Pirooznia S, Andrabi SA, Dawson VL, Dawson TM (2016) Adult conditional knockout of PGC-1 α leads to loss of dopamine neurons. *Eneuro* 3.
- Jiang Z, Rompala GR, Zhang S, Cowell RM, Nakazawa K (2013) Social isolation exacerbates schizophrenia-like phenotypes via oxidative stress in cortical interneurons. *Biol Psychiatry* 73:1024–1034.
- Kumar A, Zhang J, Tallaksen-Greene S, Crowley MR, Crossman DK, Morton AJ, Van Groen T, Kadish I, Albin RL, Lesort M, Detloff PJ (2016) Allelic series of Huntington's disease knock-in mice reveals expression discordance. *Hum Mol Genet* 25:1619–1636.
- Laforet GA, Sapp E, Chase K, McIntyre C, Boyce FM, Campbell M, Cadigan BA, Warzecki L, Tagle DA, Reddy PH, Cepeda C, Calvert CR, Jokel ES, Klapstein GJ, Ariano MA, Levine MS, DiFiglia M, Aronin N (2001) Changes in cortical and striatal neurons predict behavioral and electrophysiological abnormalities in a transgenic murine model of Huntington's disease. *J Neurosci* 21:9112–9123.
- Leone TC, Lehman JJ, Finck BN, Schaeffer PJ, Wende AR, Boudina S, Courtois M, Wozniak DF, Sambandam N, Bernal-Mizrachi C, Chen Z, Holloszy JO, Medeiros DM, Schmidt RE, Saffitz JE, Abel ED, Semenkovich CF, Kelly DP (2005) PGC-1 α deficiency causes multi-system energy metabolic derangements: muscle dysfunction, abnormal weight control and hepatic steatosis. *PLoS Biol* 3 e101.
- Lin J et al (2004) Defects in adaptive energy metabolism with CNS-linked hyperactivity in PGC-1 α null mice. *Cell* 119:121–135.
- Liu L, Ikonen S, Heikkinen T, Heikkilä M, Puoliväli J, van Groen T, Taniila H (2002) Effects of fimbria-fornix lesion and amyloid pathology on spatial learning and memory in transgenic APP + PS1 mice. *Behav Brain Res* 134:433–445.
- Lucas EK, Dougherty SE, McMeekin LJ, Reid CS, Dobrunz LE, West AB, Hablitz JJ, Cowell RM (2014a) PGC-1 α provides a transcriptional framework for synchronous neurotransmitter release from parvalbumin-positive interneurons. *J Neurosci* 34:14375–14387.
- Lucas EK, Dougherty SE, McMeekin LJ, Trinh AT, Reid CS, Cowell RM (2012) Developmental alterations in motor coordination and medium spiny neuron markers in mice lacking pgc-1 α . *PLoS One* 7 e42878.
- Lucas EK, Markwardt SJ, Gupta S, Meador-Woodruff JH, Lin JD, Overstreet-Wadiche L, Cowell RM (2010) Parvalbumin deficiency and GABAergic dysfunction in mice lacking PGC-1 α . *J Neurosci* 30:7227–7235.
- Lucas EK, Reid CS, McMeekin LJ, Dougherty SE, Floyd CL, Cowell RM (2014b) Cerebellar transcriptional alterations with Purkinje cell dysfunction and loss in mice lacking PGC-1 α . *Front Cell Neurosci* 8:441.
- Ma D, Li S, Lucas EK, Cowell RM, Lin JD (2010) Neuronal inactivation of peroxisome proliferator-activated receptor γ coactivator 1 α (PGC-1 α) protects mice from diet-induced obesity and leads to degenerative lesions. *J Biol Chem* 285:39087–39095.
- Martinez-Redondo V, Pettersson AT, Ruas JL (2015) The hitchhiker's guide to PGC-1 α isoform structure and biological functions. *Diabetologia* 58:1969–1977.
- McMeekin LJ, Li Y, Fox SN, Rowe GC, Crossman DK, Day JJ, Li Y, Detloff PJ, Cowell RM (2018) Cell-specific deletion of PGC-1 α from medium spiny neurons causes transcriptional alterations and age-related motor impairment. *J Neurosci* 38:3273–3286.
- Minichiello L, Korte M, Wolfer D, Kühn R, Unsicker K, Cestari V, Rossi-Arnaud C, Lipp HP, Bonhoeffer T, Klein R (1999) Essential role for TrkB receptors in hippocampus-mediated learning. *Neuron* 24:401–414.
- Mo A, Mukamel EA, Davis FP, Luo C, Henry GL, Picard S, Urlich MA, Nery JR, Sejnowski TJ, Lister R, Eddy SR, Ecker JR, Nathans J (2015) Epigenomic signatures of neuronal diversity in the mammalian brain. *Neuron* 86:1369–1384.
- O'Donnell KC, Lulla A, Stahl MC, Wheat ND, Bronstein JM, Sagasti A (2014) Axon degeneration and PGC-1 α -mediated protection in a zebrafish model of α -synuclein toxicity. *Dis Model Mech* 7:571–582.
- Okamoto S, Pouladi MA, Talantova M, Yao D, Xia P, Ehrnhoefer DE, Zaidi R, Clemente A, Kaul M, Graham RK, Zhang D, Vincent Chen HS, Tong G, Hayden MR, Lipton SA (2009) Balance between synaptic versus extrasynaptic NMDA receptor activity influences inclusions and neurotoxicity of mutant huntingtin. *Nat Med* 15:1407–1413.
- Pacelli C, De Rasmo D, Signorile A, Grattagliano I, di Tullio G, D'Orazio A, Nico B, Comi GP, Ronchi D, Ferranini E, Pirolo D, Seibel P, Schubert S, Gaballo A, Villani G, Cocco T (2011) Mitochondrial defect and PGC-1 α dysfunction in parkin-associated familial Parkinson's disease. *Biochim Biophys Acta* 1812:1041–1053.
- Paul A, Crow M, Raudales R, He M, Gillis J, Huang ZJ (2017) Transcriptional architecture of synaptic communication delineates gabaergic neuron identity. *Cell* 171:522–539.e20.
- Qin W, Haroutunian V, Katsel P, Cardozo CP, Ho L, Buxbaum JD, Pasinetti GM (2009) PGC-1 α expression decreases in the Alzheimer disease brain as a function of dementia. *Arch Neurol* 66:352–361.
- Rajkowska G, Selemon LD, Goldman-Rakic PS (1998) Neuronal and glial somal size in the prefrontal cortex: a postmortem morphometric study of schizophrenia and Huntington disease. *Arch Gen Psychiatry* 55:215–224.
- Ramos EM et al (2012) Population stratification may bias analysis of PGC-1 α as a modifier of age at Huntington disease motor onset. *Hum Genet* 131:1833–1840.
- Robinson A, Grösgen S, Mett J, Zimmer VC, Haupenthal VJ, Hundsdoerfer B, Stahlmann CP, Slobodskoy Y, Müller UC, Hartmann T, Stein R, Grimm MOW (2014) Upregulation of PGC-1 α expression by Alzheimer's disease-associated pathway: presenilin 1/amyloid precursor protein (APP)/intracellular domain of APP. *Aging Cell* 13:263–272.
- Rosas HD, Salat DH, Lee SY, Zaleta AK, Pappu V, Fischl B, Greve D, Hevelone N, Hersch SM (2008) Cerebral cortex and the clinical expression of Huntington's disease: complexity and heterogeneity. *Brain* 131:1057–1068.

- Saunders A, Macosko EZ, Wysoker A, Goldman M, Krienen FM, de Rivera H, Bien E, Baum M, Bortolin L, Wang S, Goeva A, Nemes J, Kamitaki N, Brumbaugh S, Kulp D, McCarroll SA (2018) Molecular diversity and specializations among the cells of the adult mouse brain. *Cell* 174:1015–1030.
- Scarpulla RC (2011) Metabolic control of mitochondrial biogenesis through the PGC-1 family regulatory network. *Biochim Biophys Acta* 1813:1269–1278.
- Schneider CA, Rasband WS, Eliceiri KW (2012) NIH Image to ImageJ: 25 years of image analysis. *Nat Methods* 9:671–675.
- Shin J-H, Ko HS, Kang H, Lee Y, Lee Y-I, Pletinkova O, Troconso JC, Dawson VL, Dawson TM (2011) PARIS (ZNF746) repression of PGC-1 α contributes to neurodegeneration in Parkinson's disease. *Cell* 144:689–702.
- Sieradzan KA, Mann DM (2001) The selective vulnerability of nerve cells in Huntington's disease. *Neuropathol Appl Neurobiol* 27:1–21.
- Sotrel A, Paskevich PA, Kiely DK, Bird ED, Williams RS, Myers RH (1991) Morphometric analysis of the prefrontal cortex in Huntington's disease. *Neurology* 41:1117–1123.
- Soyal SM, Felder TK, Auer S, Hahne P, Oberkofler H, Witting A, Paulmichl M, Landwehrmeyer GB, Weydt P, Patsch W, European Huntington Disease Network (2012) A greatly extended PPARGC1A genomic locus encodes several new brain-specific isoforms and influences Huntington disease age of onset. *Hum Mol Genet* 21:3461–3473.
- Soyal SM, Zara G, Ferger B, Felder TK, Kwik M, Nofziger C, Dossena S, Schwienbacher C, Hicks AA, Pramstaller PP, Paulmichl M, Weis S, Patsch W (2018) The PPARGC1A locus and CNS-specific PGC-1 α isoforms are associated with Parkinson's Disease. *Neurobiol Dis* 121:34–46.
- Spiegelman BM (2007) Transcriptional control of mitochondrial energy metabolism through the PGC1 coactivators. *Novartis Found Symp* 287:60.
- St-Pierre J, Drori S, Uldry M, Silvaggi JM, Rhee J, Jäger S, Handschin C, Zheng K, Lin J, Yang W, Simon DK, Bachoo R, Spiegelman BM (2006) Suppression of reactive oxygen species and neurodegeneration by the PGC-1 transcriptional coactivators. *Cell* 127:397–408.
- Su X, Chu Y, Kordower JH, Li B, Cao H, Huang L, Nishida M, Song L, Wang D, Federoff HJ (2015) PGC-1 α promoter methylation in Parkinson's disease. *PLoS One* 10 e0134087.
- Su J, Gorse K, Ramirez F, Fox MA (2010) Collagen XIX is expressed by interneurons and contributes to the formation of hippocampal synapses. *J Comp Neurol* 518:229–253.
- Szalardy L, Zadori D, Plangar I, Vecsei L, Weydt P, Ludolph AC, Klivenyi P, Kovacs GG (2013) Neuropathology of partial PGC-1 α deficiency recapitulates features of mitochondrial encephalopathies but not of neurodegenerative diseases. *Neurodegener Dis* 12:177–188.
- Taherzadeh-Fard E, Saft C, Andrich J, Wieczorek S, Arning L (2009) PGC-1 α as modifier of onset age in Huntington disease. *Mol Neurodegener* 4:10.
- Tanaka Y, Tanaka Y, Furuta T, Yanagawa Y, Kaneko T (2008) The effects of cutting solutions on the viability of GABAergic interneurons in cerebral cortical slices of adult mice. *J Neurosci Methods* 171:118–125.
- Thau N, Knippenberg S, Körner S, Rath KJ, Dengler R, Petri S (2012) Decreased mRNA expression of PGC-1 α and PGC-1 β -regulated factors in the SOD1G93A ALS mouse model and in human sporadic ALS. *J Neuropathol Exp Neurol* 71:1064–1074.
- Török R, Kónya JA, Zádori D, Veres G, Szalárdy L, Vecsei L, Klivenyi P (2015) mRNA expression levels of PGC-1 α in a transgenic and a toxin model of Huntington's disease. *Cell Mol Neurobiol* 35:293–301.
- Wareski P, Vaarmann A, Choubey V, Safulina D, Liiv J, Kuum M, Kaasik A (2009) PGC-1 α and PGC-1 β regulate mitochondrial density in neurons. *J Biol Chem* 284:21379–21385.
- Weydt P, Pineda VV, Torrence AE, Libby RT, Satterfield TF, Lazarowski ER, Gilbert ML, Morton GJ, Bammler TK, Strand AD, Cui L, Beyer RP, Easley CN, Smith AC, Krainc D, Luquet S, Sweet IR, Schwartz MW, La Spada AR (2006) Thermoregulatory and metabolic defects in Huntington's disease transgenic mice implicate PGC-1 α in Huntington's disease neurodegeneration. *Cell Metab* 4:349–362.
- Weydt P, Soyal SM, Gellera C, Didonato S, Weidinger C, Oberkofler H, Landwehrmeyer GB, Patsch W (2009) The gene coding for PGC-1 α modifies age at onset in Huntington's Disease. *Mol Neurodegener* 4:3.
- Weydt P, Soyal SM, Landwehrmeyer GB, Patsch W, European Huntington Disease Network (2014) A single nucleotide polymorphism in the coding region of PGC-1 α is a male-specific modifier of Huntington disease age-at-onset in a large European cohort. *BMC Neurol* 14:1.
- Williams SR, Stuart GJ (1999) Mechanisms and consequences of action potential burst firing in rat neocortical pyramidal neurons. *J Physiol (Lond)* 521:467–482.
- Zheng B et al (2010) PGC-1 α , a potential therapeutic target for early intervention in Parkinson's disease. *Sci Transl Med* 2:52ra73.

APPENDIX A. SUPPLEMENTARY DATA

Supplementary data to this article can be found online at <https://doi.org/10.1016/j.neuroscience.2020.03.036>.

(Received 15 July 2019, Accepted 21 March 2020)
(Available online 25 March 2020)